ISOTOPIC FRACTIONATION IN SPUTTERING

Thesis by
Stephen James Spicklemire

In Partial Fulfillment of the Requirements
for the Degree of
Doctor of Philosophy

California Institute of Technology
Pasadena, California

1990
(Submitted January 5, 1990)

Acknowledgments

I wish to thank everyone who either directly, or indirectly, made this work possible. I am grateful to my advisor, Tom Tombrello, without whose encouragement and support I could have never completed this project. Thanks are certainly due to the indefatigable Duncan Weathers, for his countless hours of labor, his unlimited supply of enthusiasm, his neat TEX macros and the figures for Chapter 2. I am indebted to G. J. Wasserburg for the use of the PANURGE ion probe and the generous assistance of Ian Hutcheon in operating and maintaining the instrument during the course of this work. I would like to thank Kevin Hubbard for the use of his In:Ga collectors and I wish to acknowledge the considerable effort of Hide Suzuki in helping with the final measurements.

Among the others who made substantial contributions to my overall graduate school experience I must express my sincere and deep appreciation for the friendships of Alan Rice and Shouleh Nikzad. They made, what could otherwise have been at times, a rather gloomy existence, downright enjoyable. I would like to thank Michelle Vine for her skilled assistance with countless administrative details, and for many interesting contributions to our 'group discussions.' I am also grateful to Steve Stryker for his patient guidance in the machine shop and I thank the rest of the Brown Bag crew, present and past, for their friendship and encouragement. I wish to thank Don Burnett and Dorothy Woolum for providing some additional interesting problems to think about and for their generous support. I am further indebted to Tim and Barbara Zukowski for their generous hospitality during my stays in Southern California, and for a most enjoyable friendship. Thanks are also due the faculty and staff of the University of Indianapolis for their patience and support. Also I would like to thank Carl Calabria and the folks at Truevision Inc. for the ATVista(tm) graphics card which has proven very helpful in visualizing the simulation results and for the various consulting opportunities they have provided.

I must also acknowledge three individuals, who perhaps more than any others, fueled my interest in Physics. The first is my undergraduate advisor, Mike Moloney, who to this day, keeps me on my toes by posing various puzzles and problems. The second is my high school physics teacher, Richard Hammond, whose encouragement and guidance I shall always value. The third is Kevin Friedly, who not only helped with proofreading of this thesis, but also encouraged and supported my throughout my graduate school career and continues to provide stimulating ideas and very interesting discussions.

I thank my parents, and the rest of my family, for providing the kind of emotional and intellectual support that has allowed me to do these things. Finally, for her understanding, flexibility, companionship, encouragement, and unquestioning love I dedicate this thesis to Sherri, my wife.

Abstract

Isotopic fractionation due to sputtering has been investigated via a collector type experiment in which targets of known isotopic composition have been bombarded with several keV Ar^+ and Xe^+ ions with fluences down to 3.0×10^{14} ions/cm^2, believed to be the lowest fluences for which such detailed measurements have ever been made. The isotopes were sputtered onto carbon collectors and analyzed with Secondary Ion Mass Spectroscopy (SIMS.) There is clear indication of preferential effects several times that predicted by the dominant analytical theory. Results also show a fairly strong angular variation in the fractionation. The maximum effect is usually seen in the near normal direction, measured from the target surface, falling continuously, by a few percent in some cases, to a minimum in the oblique direction. Measurements have been made using Mo isotopes: ^{100}Mo and ^{92}Mo and a liquid metal system of In:Ga eutectic. The light isotope of Mo is found to suffer a 53 ± 5‰ (note: 1.0 ‰ $\equiv$ 0.1%) enrichment in the sputtered flux in the near normal direction, compared to the steady state near normal sputtered composition, under 5.0 keV Xe^+ bombardment of 3.0×10^{14} ions/cm^2. In the liquid metal study only the angular dependence of the fractionation could be measured due to the lack of a well defined reference and the nature of the liquid surface, which is able to 'repair' itself during the course of a bombardment. The results show that ^{113}In is preferentially sputtered over ^{115}In in the near normal direction by about 8.7 ± 2.7‰ compared to the oblique direction. ^{69}Ga, on the other hand, is sputtered preferentially over ^{71}Ga in the oblique direction by about 13 ± 4.4‰ with respect to the near normal direction.

Table of Contents

List of Figures

List of Tables

Chapter 1

Overview of the Sputtering Process

1.1 Sputtering by keV Ions

Sputtering is a phenomenon that has been known for some time [1],[1.1] although it has only come under intense scrutiny during the past couple of decades. It is essentially a form of surface erosion associated with the bombardment of a surface by energetic particles. This encompasses a rather large class of experimental situations from the erosion of filaments and other exposed surfaces in gaseous discharge tubes (e.g., the original observation by Grove) to the sputtering of solar system material exposed to the solar wind [2]. Various modern analytical techniques use sputtering either as a primary tool, (e.g., Secondary Ionization Mass Spectroscopy (SIMS) and Secondary Neutral Mass Spectroscopy, (SNMS) [3]) or simply as a method for removing surface material to make depth profiles of various measurable surface characteristics, (e.g., Auger Electron Spectroscopy (AES) [3].) In addition there are several technological applications for sputtering, such as sputter film deposition and ion beam milling for micron sized "mechanical" structures. [4]

The sputtering we will describe in this work will exclusively involve the bombardment of multicomponent and possibly inhomogeneous metal surfaces with ions in the keV energy range. This restricts the possible mechanisms that can reasonably be held accountable for sputtering. The most appropriate model to describe this regime is the 'dilute collision cascade' [5,6]. This picture suggests that the incident ion is acted on by a series of electronic and nuclear collisions that reduce its energy as it travels through the material. The nuclear component of these collisions naturally causes the atoms of the material to move and undergo still further collisions, hence the term 'collision cascade.' Ultimately this collision sequence results in some number of atoms, molecules, clusters or 'chunks' to be emitted from the surface and

[1.1] It was first observed by W.R. Grove, as reported in 1853.

hence 'sputtered.' The 'dilute' term refers to the assumption that, for the most part, atoms set in motion have collisions only with atoms that are at rest. The violation of this assumption amounts to entrance into the so-called 'spike' regime [5]. This generally occurs at higher energies or for heavier ions than used in these experiments.

1.2 Characterization of Sputtering: The Sputtering Yield

The most easily measurable quantity associated with sputtering is the *sputtering yield*, Y. It is defined to be the number of sputtered particles per incident particle. In the low current and keV energy range used in these investigations this ratio is constant for any given target composition, independent of the ion flux.[1.2] The yield can be decomposed in any number of ways into partial or differential sputtering yields (e.g., with respect to the species of the sputtered particles, their angle of emission, their depth of origin, their energy, etc.).

In the following discussion the quantities of interest are the relative sputtering yield of one component of the solid compared to some other component measured as a function of angle from the surface normal and primary ion beam dose. The notation used here will be:

$$\frac{\partial Y_a}{\partial \Omega}(\theta) / \frac{\partial Y_b}{\partial \Omega}(\theta), \tag{1.1}$$

where a and b denote separate species present in the solid being sputtered. Naturally the total sputtering yield is the sum of all the partial yields for all species integrated over all solid angles Ω.

1.3 Sputtering of Multicomponent materials

We will see that the partial sputtering yields for the species in the solid are not simply proportional to their respective concentrations in the solid. Some components are enriched in the sputtered flux or *preferentially* sputtered. The notation

[1.2] Of course if the target composition changes, due the ion *fluence*, then the yield may change in response.

used in this work to describe this effect is the following:

$$\delta_{ij} = \left(\frac{Y_i/Y_j}{c_i/c_j} - 1 \right) \times 1000, \tag{1.2}$$

where δ_{ij} is sometimes called the *enrichment*, Y_i and Y_j are the sputtering yields for the components i and j and c_i and c_j are the concentrations of the components i and j, in the bulk material being sputtered. The factor of 1000 indicates that δ_{ij} is normally expressed as parts per thousand or '‰.' Clearly if $\delta_{ij} > 0$ then component i is enriched with respect to component j in the sputtered flux compared to their respective concentrations in the bulk sample. This naturally induces changes in the composition of the sample near the surface[1.3], and as a result the partial sputtering yields are a function of ion beam *fluence.* It is clear therefore that if accurate measurements of the enrichment effect are to be made, they must be made in the *low fluence limit.* This demands a low primary ion beam dose and hence a high degree of sensitivity in any detection method used to measure the sputtered material.

In the experiments described in this work the 'components' whose sputtering yields are compared are all isotopes of the same element. This is done so that any chemical effects, which are surely present in the general case of multicomponent sputtering, will be absent. Unfortunately this restricts these experiments to systems with fairly small relative mass difference (e.g., $\delta M/M \leq 10\%$) between the components under study. This obviously limits the magnitude of the preferential effects we can generate and underscores the need for an analytical technique that is both sensitive and precise.

Before launching into a detailed description of these experiments it is worthwhile to peruse the results obtained by other investigators. Below are listed some results of studies of other researchers relevant to the issue of isotopic fractionation in sputtering. The nature of the isotopic systems studied varies fairly widely both in the composition of the target materials and the identity of the bombarding species.

[1.3] At least this is the case while sputtering a solid target. We will discuss exceptions to this in chapter 4 when considering preferential sputtering of liquid targets.

The most important issue though is probably the lowest bombarding fluence used in a measurement. In general, large bombarding fluences have been used, which cause the measured fractionation to be rather small in most cases. The recent measurements of Gnaser[7,8] are an exception to this rule and compare quite favorably to the results of these studies.

Table 1.1 Some Results of Previous Investigations

Target	Bombarding Ion	i	j	$\delta_{ij}‰$	fluence ions cm^{-2}	Ref.
Li	5 keV Ar^+	^6Li	^7Li	17	5.3×10^{16}	[9]
Li	20 keV Ar^+	^6Li	^7Li	19	5.3×10^{16}	[9]
$CaAl_2Si_2O_8$	130 keV N_2^+	^{40}Ca	^{44}Ca	21.2	5.8×10^{17}	[10]
$Ca_5(PO_4)_3F$	100 keV N^+	^{40}Ca	^{44}Ca	11.5	1.2×10^{17}	[10]
CaF_2	100 keV N^+	^{40}Ca	^{44}Ca	12.7	1.3×10^{17}	[10]
Mg	2 keV He^+	^{24}Mg	^{25}Mg	≥ 10.3	$10^{17} - 10^{18}$	[11]
Cu	13.2 keV O^-	$^{63}Cu^+$	$^{65}Cu^+$	8	—	[12]
$LiAlSi_2O_6$	14.5 keV O^-	$^6Li^+$	$^7Li^+$	53	$\sim 10^{15}$	[13]
LiF	14.5 keV O^-	$^6Li^+$	$^7Li^+$	53	$\sim 10^{15}$	[13]
TiO_2	14.5 keV O^-	$^{48}Ti^+$	$^{50}Ti^+$	37	$\sim 10^{15}$	[13]
GaAs	14.5 keV O^-	$^{69}Ga^+$	$^{71}Ga^+$	12	$\sim 10^{15}$	[13]
Mo	14.5 keV O^-	$^{92}Mo^+$	$^{100}Mo^+$	49	$\sim 10^{15}$	[13]
B	100 keV Ne^+	$^{10}B^+$	$^{11}B^+$	46	$\sim 10^{15}$	[14]
B	100 keV Ar^+	$^{10}B^+$	$^{11}B^+$	52	$\sim 10^{15}$	[14]
Mo	5 keV Ar^+	^{92}Mo	^{100}Mo	52	$\sim 10^{15}$	[7,8]
Ge	5 keV Ar^+	^{70}Ge	^{76}Ge	51	$\sim 10^{15}$	[7,8]

The latest data available suggest that, at the lowest bombarding fluences available, the degree of fractionation can become $\sim$ 5 %. We will see that the above measurements are consistent with the measurements in this study taken at the lowest fluences yet. The other aspect of istopic fractionation that this study dramatically clarifies is the degree to which the low fluence isotopic fractionation can

depend on angle. There is very little data available on angular dependence. Russell *et al.* [10] made a measurement of the angular dependence of δ ($^{40}Ca/^{44}Ca$) by measuring the istopic composition of sputtered material ejected into polar angular ranges 5–25°, 25–41°, and 41–72°. The fractionation δ ($^{40}Ca/^{44}Ca$) was found to be 13.3‰, 17.3‰, and 8.0‰ for a fluorite (CaF_2) target bombarded with $\sim 1.3 - 2.4 \times 10^{17}\,cm^{-2}$. This angular fractionation is observed to persist even when the overall isotopic composition of the sputtered flux is equal to the bulk composition of the target.

Chapter 2

Experimental Methods

2.1 The Sputtering Experiments

The first stage of the experiments consisted of bombarding targets of known isotopic composition, thereby sputtering the target material onto carbon collectors maintained in a well defined geometry.

2.1.1 The In : Ga Sputtering

The In : Ga sputtering was performed at Yale University by Dr. Kevin Hubbard. The conditions of these bombardments are very similar to those for the ^{92}Mo : ^{100}Mo experiments. The important differences will be discussed in chapter 4.

2.1.2 The Mo Sputtering

In the ^{92}Mo : ^{100}Mo experiments the sputtering took place in the target room of the Caltech 6MV (million volt) Van de Graaff Tandem Accelerator. The geometry of the target chamber in relation to the keV accelerator and the 6MV machine is rendered in figure 2.1. This station was originally designed so MeV and keV ions could be used in one experiment *in situ*. The keV accelerator consisted of an RF (radio frequency) ion source connected to a short accelerating column followed by focusing and steering optics including a 90 degree double focusing sector magnet, which was used to momentum analyze the ions. There were additional focusing and steering optics just upstream from the target chamber. The targets were mounted in an ion pumped UHV (ultra high vacuum) chamber immediately following an in line LN_2 cold trap. The ultimate pressure of the target chamber was typically $\sim 10^{-9}$ Torr without beam. When the ion beam was directed into the target chamber the pressure rose to ~ 1 to 5×10^{-8} Torr; however this pressure was probably dominated

by the noble gas used in the ion source to provide the incident ions and would have little effect on the sputtering process.[2.1] Both Xe^+ and Ar^+ were used to bombard the targets, one (Ar) lighter than Mo and one (Xe) heavier. The energies of the bombarding ions were selected as 5keV and 10keV. The ion optics become difficult much below 5keV while the 90 degree magnet was incapable of bending anything more energetic than 10keV Xe^+. The ion beam was rastered over the target surface during the bombardment to insure a uniform dose. Typical rastering frequencies were several Hz for one direction and a fraction of a Hz for the other. Bombardment times were as long as several hours for large doses, and never less than $\sim$ 5 min. even for the lowest dose runs.

The targets were $\sim 5\,\mathrm{mg./cm.^2}$ Mo foil manufactured at Oak Ridge National Laboratory to have a 1:1 ratio (50 atomic percent each) of ^{92}Mo and ^{100}Mo with only trace concentrations of the other stable Mo isotopes. The large 80‰ mass difference was intended to accentuate any mass effect present in the sputtering of the foils.

The foils were etched in a 1:1 mixture of HCl and H_2O_2 diluted with deionized water then rinsed with isopropanol and warm air dried prior to being loaded into the target chamber. Once loaded and evacuated to $\sim 1 \times 10^{-6}$ Torr the chamber was baked for 24 hours at 300 C° after which the base pressure in the chamber fell to $\sim 1 \times 10^{-9}$ Torr.

During the bombardment the targets were held at an elevated temperature of 150 $\pm$1C°, which helped to maintain a relatively clean surface. The geometry of the interior target chamber is depicted in figure 2.2. The collectors were carbon sheets several mils thick, and were held inside a right cylinder of circular cross section. There were $\sim$ 0.25 in. holes along the length of the foil holder that allowed the beam to pass through to the targets. Corresponding holes were cut in the carbon foils making the minimum angle for which sputtered material could be measured

[2.1] See appendix A for a discussion of various issued related to vacuum requirements and surface cleanliness in surface analysis.

$\sim$ 15° from the normal direction. The collector assembly was electrically isolated so that an estimate of charge sprayed from the target (e.g. secondary electrons and ions) could be made. Currents through the collector were typically $\sim$ 1/10 of the target current and were electronically summed with the current flowing down the target holder to achieve correct beam current integration.

Upstream from the target there were several collimators that defined the beam geometry and provided secondary electron suppression voltages used to insure accurate charge integration at the target. The total integrated charge on the target and the collector foils was then used to calculate the total beam dose over the rastered area. The rastered beam spot size was measured by bombarding a Ti film on a stainless steel substrate, that left clearly visible damage from the beam spot. It was found to have an area of $0.62\,\mathrm{cm}^2$.

The procedure was to first bombard a target to a predetermined dose, the beam was then temporarily chopped with a butterfly valve and the collector assembly was moved so that a pristine collector surface was presented before the target. (Because each collector surface had its own beam hole, there was no difficulty getting beam consistently delivered to the target.) The positions of the collection regions were determined carefully to be very nearly 0.460 inches apart and the manipulator used to position the collectors was accurate to about 0.001 inches. When the new collector was in place, the beam was admitted to the target chamber and the next dose began. This process was repeated until the maximum dose for that particular target was achieved. For the lowest dose runs several targets were sputtered onto the same collector region to accumulate a measurable amount of Mo. The time during which the beam was turned off was kept as small as possible in order to avoid contamination of the surface (see appendix A). This time never exceeded one minute.

Ultimately the collectors were removed from the target chamber and cut into small samples that could be conveniently analyzed using the PANURGE ion microprobe. This was accomplished using a custom 'jig' that allowed careful alignment

of the collectors and maintained fixed registration so that angular positions of the collector surface could be repeatably positioned on the sample holder of the microprobe. Positioning repeatability was determined to be $\sim \pm 50\mu$ with moderate care in aligning the samples.

2.2 Measuring Isotopic Ratios using SIMS

The analysis of the foils was carried out at the Caltech PANURGE ion microprobe (a modified Cameca IMS-3f)[15]. The collector sections from the original sputtering experiment were bombarded with ions of O_2^+ and O^- accelerated through potential drops of 10.5 kV and −17.0 kV respectively. Typical beam currents were in the range of 5 to 10 nA. The incident beam was directed roughly 30° from the sample normal and was focused to a diameter of several microns. The resulting beam spot was rastered over a 100 μ area on the collector surfaces. Secondary ions leaving the surface of the samples (e.g. $^{100}Mo^+$, $^{92}Mo^+$, $^{71}Ga^+$, $^{69}Ga^+$, $^{115}In^+$, $^{113}In^+$) within a 60 μ diameter circle centered on the rastered area and within $\sim 15°$ of the sample surface normal were further accelerated through a 4.5 kV drop and were then focused and energy analyzed to eliminate the long high energy tail, a normal characteristic of the collision cascade. Next they were momentum analyzed in a high precision magnetic sector with entrance and exit slits adjusted to provide an overall mass resolution $M/\Delta M$ of $\sim$ 500. This resolution is consistent with the conditions of these experiments, having no separable isobaric interferences to eliminate. While the instrument is capable of much higher resolution measurements (e.g., $M/\Delta M \sim 10000$), this invariably reduces the transmission of the machine, significantly increasing the time required to make a measurement. A much higher resolution *was* used to investigate quantitatively the isobaric background for the measurements presented here.

Once analyzed, the ions could be 1) selectively focussed on a microchannel plate and provide either an image of the sample surface or an image of the beam profile passing through the slits of the magnetic sector, or 2) deflected before the microchannel plate and sent to an electron multiplier to be counted. The microprobe

runs under the control of an HP9845B workstation via an IEEE-488 bus connected to all the relevant power supplies and meters/instruments.

During the course of measuring one area on a collector section (typically requiring about an hour) the secondary ion count rate might fall by a factor of 2 or 3 simply due to the sputtering of the collected material from the sample surface. Unfortunately *both* isotopes of interest are sputtered away in this process, meaning that a second isotope can't be measured after the measurement of the first is complete. Another difficulty is that the magnet can drift a small amount over the course of an hour, shifting the mass peak out of the exit slits. Both of these problems are eliminated by using the computer to cycle the magnet current periodically back and forth between the mass peaks of interest. At each peak the count rate is measured at the center and sides of the peak. The count rate at the sides of the peak is used to compensate for any current drift in the magnet, effectively keeping the peak centered on the exit slits of the analyzer. The count rate at the center of the peak is stored and represents the 'size' of the peak at the time of the measurement. The time used to measure each peak was generally between 3 and 10 seconds giving complete cycle times of 15 or 20 seconds.

The sequence of peak sizes for a particular area was used to calculate the relative isotope ratio of the two isotopes measured for that area of the collector.[2.2] Because each area of the collectors corresponds to a different angle with respect to the surface normal in the original sputtering experiment, we get a picture of how the isotopic ratio depends on ejection angle in the original experiment.

The term 'relative isotope ratio' used above requires explanation. It is a well known fact that SIMS analysis has an *inherent* fractionation effect[12, 16-18]. The isotope ratio, as measured directly here, does not reflect the *true* isotope ratio of the material sputtered onto the collector surface. The secondary ion sputtering yield has a dependence on the ejection velocity of the sputtered ion, essentially related to the time the ion spends near the surface as it departs[12,19]. In this work, all

[2.2] See appendix B for a detailed account of this calculation.

of the isotopic fractionations are reported with respect to the near normal angle (determined by target/collector geometry) at the highest beam fluences available. In the case of ^{92}Mo:^{100}Mo this corresponds to the 5.0 keV Xe^+ bombardment at $\sim 20 \times 10^{-15}$ cm^{-2}. We will see in chapter 4 that when sputtering a liquid target, the fluence is irrelevant to the isotopic fractionation of the sputtered material. This means that, in the In–Ga experiments we can only measure the zero fluence limit of the relative fractionation of the In and Ga isotopes as a function of ejection angle.

In performing the SIMS analysis some concerns developed regarding the accuracy of the results. It had been observed previously that Heavy Ion Rutherford Backscattering (HIRBS) analysis of the foils was very difficult due to unusually long, low energy 'tails' in the HIRBS spectra.[20] These tails could be a result of the relatively 'rough' nature of the machined carbon foil surfaces. On the other hand, it is also possible that the Mo could have diffused into the carbon foil, giving 'tails' from the depth profile of diffused Mo. This could be a problem in SIMS analysis because the diffusion depth would be mass dependent, resulting in a dependence of the isotope ratio on time during the SIMS analysis. Another effect that was watched for was 'secondary preferential sputtering.' Because there were two isotopes on the collectors it seemed plausible that they *might* suffer from a preferential sputtering effect similar to the one we were trying to measure from the original metal surface. To the degree that this secondary preferential sputtering was constant, it was not an issue, because it would be corrected along with any other overall instrumental fractionations, when the results were normalized as outlined above. During the vast majority of SIMS measurements there was no indication of any systematic trend in the isotope ratio over time. However, there were several instances where an unusual 'hot spot' was discovered on the collectors that had an isotopic ratio that was 1) unusually high compared to the measured isotope ratio in the vicinity (e.g., 150.0 μ in any direction from the hot spot) and 2) became systematically higher the longer the SIMS analysis progressed. The locations could be re-analyzed at any time with essentially the same result. These points are currently suspected to be the result of

contamination of the either the collectors or the targets with some of the pure ^{92}Mo used in a related experiment. This seems surprising in view of the considerable precautions taken to avoid such a contamination. Fortunately they do seem to have a characteristic signature and can be fairly easily identified and eliminated from the data at the outset.

There is also evidence that the surface of the Mo samples was at least partially oxidized before the bombardment. This is not entirely surprising because they were exposed to air as they were loaded into the target chamber. Rutherford Backscattering analysis of the collector foils has indicated that the sputtering yield of the Mo isotopes increased by about a factor of 2 during the bombardment. This can be explained by assuming that the oxygen on the surface of the Mo was sputtered preferentially and as it was sputtered away, the relative yield of Mo increased. TRIM[28] calculations were performed that indicate that it would only require $\sim 25\%$ coverage of O to reduce the Mo sputtering yield by a factor of 2. As the O is sputtered the yield of Mo presumably goes up to its 'clean' surface value. It is difficult to determine the precise effect this might have on the isotopic fractionation. There is evidence that the isotopic fractionation is relatively insensitive to the chemical matrix of the solid[10], however it is not immediately clear how this should be understood theoretically (e.g., see chapter 5). In any case the presence of O at the surface is indicated and should be kept in mind when interpreting these results.

Chapter 3

Preferential Sputtering of Mo Isotopes

3.1 Dependence on Dose

In general the fractionation of the sputtered material depends both on angle and ion beam fluence. As the ion beam bombards the sample, the near surface isotopic composition changes as a result of preferential sputtering of the lighter isotope. The surface becomes depleted in the lighter isotope and enriched in the heavier isotope. This process continues until a steady state isotopic depth profile develops. In the steady state, the sputtered material has a composition, which, when integrated over all solid angles, matches the isotopic composition of the bulk sample. However, the isotopic composition of the sputtered material is observed to continue to have a dependence on ejection angle even in the limit of infinite ion beam fluence.

As was mentioned in chapter 2, all of the isotope ratios presented in this work are actually relative isotope ratios compared to the ratio from the near normal direction of the original sputtering geometry at the highest ion beam fluences available. In the case of Mo isotopes this corresponds to the ratio of ^{92}Mo to ^{100}Mo under 5.0 keV Xe^+ bombardment at a fluence of $\sim 20 \times 10^{-15}\,cm^{-2}$. This ratio will be referred to as R_{ij}^{STD}. At the lowest fluence measured in this study, $.3 \times 10^{15}\,cm^{-2}$, (believed to be the lowest fluence for which such data has *ever* been obtained) under bombardment by 5.0 keV Xe^+, the lighter isotope ^{92}Mo was sputtered preferentially with $\delta_{ij} \sim 53 \pm 5‰$. As the dose increased the relative fractionation fell. At a dose $3 \times 10^{15}\,cm^{-2}$, the relative fractionation was only half its low dose value.[3.1]

[3.1] A complete set of all the results of this study can be found in tabular form in Table 3.1. Most of these data are new, although some have been presented previously: Weathers, D.L., Ph.D. Thesis, California Institute of Technology, May, 1989.

Figure 3.1 shows the fractionation of the Mo isotopes as a function of ion beam fluence measured in the near normal direction under bombardment of Ar^+ and Xe^+ ions with energies of 5.0 keV and 10.0 keV respectively. Note that except for the case of 10.0 keV Xe^+, the relative composition of the sputtered material goes to ~ 1.0 in the limit of 'infinite' fluence. This is an indication that the high dose, near normal estimate of the steady state composition R_{ij}^{STD} is close to a true steady state value. The 10.0 keV Xe^+ ratio appears to be falling still at the highest fluence measured, suggesting that it too might eventually reach ~ 1, given a large enough dose. In any case our value of R_{ij}^{STD} is, if anything, low. This means ratios calculated using our experimental R_{ij}^{STD} will be inherently conservative. Furthermore, because we are measuring relative to the near normal we are also *underestimating* the absolute fractionation effect compared to the bulk ratio because, in the steady state, it is the integrated sputtered composition that is equal to the bulk ratio, not the composition in the normal direction. As we will see, the theoretical fractionation δ_{ij}^{th}, (i.e., δ_{ij} compared to the true bulk composition, as opposed to our experimentally determined R_{ij}^{STD}) is largest in the near normal direction for 5.0 keV Xe^+, and remains non-zero there, even in the infinite fluence limit. Finally the 'fluence range', over which the fractionation changes significantly, is also nearly the same for both energies of a given ion species. Clearly these systems are all qualitatively similar, at least as far as dose dependence is concerned. At low doses the lighter isotope is preferentially sputtered with a fractionation of 30 to 50‰ until, after $\sim 2 \times 10^{16}$ ions/cm^2 or so, the overall fractionation goes essentially to zero.

3.2 Dependence on Angle

Figures 3.2 through 3.8 show the angular dependence of the relative isotope ratios of ^{92}Mo compared to ^{100}Mo relative to the standard R_{ij}^{STD}, for a series of doses and ion/energy combinations. The most thoroughly investigated case was that of 5.0 keV Xe^+. The effects here were large, meaning that a statistically meaningful conclusion could be drawn with a reasonably short experiment.

The general trend in the data in the 5.0 keV Xe^+ case is that the fractiona-

tion goes down at higher angles from the surface normal. The effect clearly *doesn't* disappear as the primary ion beam dose is decreased. In fact, it seems that additional ion beam dose has the sole effect of *'sliding'* the whole curve down by about 50‰ in the infinite fluence limit. The shape of the curve does appear to change somewhat at *very* high fluence. This might be due to changes in surface topology as a result of ion beam damage. There is evidence, namely Heavy Ion Rutherford Backscattering data, indicating that the surface of the samples was suffering from some modification in the high fluence runs [20]. Some sharp angular features are therefore not entirely surprising in these instances. At any given fluence there is $\sim$ 25‰ difference between the isotopic ratios measured near the normal and far from the normal direction. The other ion/energy combinations produce results that are not altogether different from the 5 kev Xe^+ case. In general the fractionation falls with dose and, with the exception of the low dose 10 keV Ar^+, the fractionation falls somewhat with the angle from the normal directon. It will be seen in chapter 5 that these results stand in fairly sharp contrast with the predictions of most analytical theories, and are in at least partial agreement with other computer simulation efforts [21-23].

Chapter 4

Sputtering of Ga/In Isotopes from the Eutectic Alloy

4.1 Issues Involved in Sputtering from a Liquid Target

The possibility of sputtering from a liquid target holds special interest in a study of fractionation because of the ability of a liquid surface to 'repair' itself, under all but the most intense bombardments, to the degree that it appears forever undamaged. A typical self diffusion constant for a liquid metal near its melting point is 10^{12} Å^2/s. Typical incident ion beam current densities are 1 μA/cm^2 or $\sim 10^{12}$ions/(cm^{2}s) for these studies. Damage cross sections are typically on the order of 10^{-14} cm^2 indicating that the timescale for two collisions in the same region of impact is $\sim$ 100 s. Given the large self-diffusion constants for liquid metals it seems clear that isotopic equilibrium should be maintained in the surface layer as long as the bulk ratio of isotopes is fixed. A sufficiently long bombardment might deplete the bulk sample of a particular isotope, but this is not an issue as long as most of the sample remains unsputtered. (From the conditions used in this study it would take on the order of 10^{10} s or $\sim$ 300 years to reach such a condition.) As a result, sputtering of a liquid metal target is essentially equivalent to the extreme *low fluence limit* of sputtering from a solid target. Given the efforts required to make meaningful measurements at low fluence in the Mo system this is a profound improvement.

Another distinctive feature of sputtering from a liquid target is that the surface may be easily cleaned prior to the collection experiment by sputtering any impurities away without regard to possible damage to the surface. The presence of oxides or other contaminants can be largely eliminated from consideration. This is also in sharp contrast with the solid target experiment where preparing a clean initial target surface without modifying the isotopic composition is problematic.

There is a particularly interesting issue associated with the structure of liquid In:Ga eutectic. There is a built in inhomogeneity in the In:Ga system due to an effect known as Gibbsian segregation[24]. There is a large reduction in the free energy of In when it sits on the surface, compared to its value in the bulk liquid[24]. This has the remarkable effect of rendering the surface layer of the liquid extremely enriched in In compared to the bulk composition. Experiments by Dumke[24], and Hubbard[25], have shown that the surface composition is $\sim$ 96% In, while in the bulk In consists of only $\sim$ 9.7% of the overall composition. This has two effects on the sputtering yields of In and Ga: 1) In is sputtered with a much higher yield than one would expect from the composition in the bulk, and 2) the angular distributions of sputtered In and Ga atoms are very different, with In having a roughly $Y_{In} \sim \cos^{1.8}(\theta)$ dependence and Ga falling off much more sharply $Y_{Ga} \sim \cos^{3.2}(\theta)$.

These factors play a role in the analysis of the collectors for isotopic fractionation. Because there is no change in the surface isotopic composition with dose we cannot normalize the In:Ga results in the same fashion as was done in the Mo case. There, the largest dose run was used as the standard against which all other isotope ratios were measured. The idea being that after a sufficiently large dose, the integrated sputtering yield must represent the bulk composition as a result of changes in the *near surface target composition*. For the liquid target, the sputtering yield is essentially dose independent meaning that there is no reliable reference to compare the SIMS data to in order to calculate the absolute isotopic ratio of sputtered flux. As a result the only meaningful measurement that can be made is that of the *relative* fractionation of the In:Ga isotopes with respect to angle. The angular dependence of the fractionation of the In and Ga isotopes is given below. All measurements are made *relative* to the unknown fractionation of the isotopes at the near normal direction ($\sim 6°$.) The fractionation data for Ga isotopes is also limited to about 70° from the normal direction due to the sharp decrease of Ga coverage on the collectors at large angles, a result of the corresponding sharpness of the Ga sputtering yield as a function of emission angle. It was also discovered that

there was a significant concentration of Cr on the surface of the collector near the normal direction presumably due to the sputtering of stainless steel by some stray beam. Natural Cr is about 84% ^{52}Cr and 9.5% ^{53}Cr. This means that $^{53}Cr^{16}O$ can interfere with ^{69}Ga. The amount of ^{53}Cr was determined indirectly by measuring the ^{52}Cr and assuming approximately natural abundances of the other isotopes. Although the amount of interfering Cr was very small (about 2‰ in the near normal direction and much less at the higher angles used), a correction was made accounting for the interference in the results presented here. (The background was smaller than the statistical uncertainty of the measurements.)

4.2 Angular Dependence of the Isotopic Composition

The experimental conditions for the initial sputtering experiment of the liquid In:Ga system were very similar to those for the Mo system, except that the ion beam energies were generally somewhat higher (25.0 keV Ar^+), and the physical size of the carbon collectors was larger (radius of collector cylinder $\sim$ 3.64 cm), allowing the near normal measurements to approach within $\sim 5°$ of the normal direction. The SIMS analysis of the collectors was identical to the Mo study.

Figure 4.1a shows the dependence of the ratio of ^{113}In to ^{115}In as a function of angle from the target normal. The dependence is similar to that in Mo except that the effect is much smaller. This is expected in view of the relatively small mass difference. The result for Ga is quite interesting. Figure 4.1b shows the dependence of the ratio of ^{69}Ga to ^{71}Ga as a function of angle from the target normal. Unlike the Mo and In fractionation the Ga seems to prefer the heavy isotope at higher angles. One might speculate that since the Ga has to traverse a layer of In to be sputtered (presumably the cause of the sharp reduction of Ga at high angles) and the effective thickness of that layer grows as $\sim \sec(\theta)$ that the lighter mass is more effectively transmitted through the layer than the heavier due to its smaller differential cross section.

Chapter 5

Theoretical Understanding of Preferential Sputtering

5.1 Predictions of Analytical Theory

The most dominant, and largely successful, theory of sputtering is that due to Sigmund[26]. This theory results from the linearization of a modified Boltzmann equation in the 'dilute cascade limit'. This is a reasonable approximation if the density of the cascade is low, (i.e., moving atoms rarely collide with atoms previously set in motion), but still contains many atoms. Sputtering is treated in this framework by embedding a mathematical surface in the bulk of the cascade and calculating the flux of particles moving across it, taking into account the surface binding energy, which prevents low energy recoils from being sputtered. To first order in the mass difference, this theory predicts that the effect of preferential sputtering comes entirely from the relative differential cross sections for collisions between the light and heavy isotopes. In particular the light isotope is predicted to be enriched *isotropically* in the sputtered flux by a factor of:

$$(M_i/M_j)^{2m}, \tag{5.1}$$

where m is the characteristic exponent from the differential cross section,

$$d\sigma_{ij}(E,T) \approx C_{ij}E^{-m}T^{-1-m}, \quad 0 < T \leq \gamma_{ij}E, \tag{5.2}$$

appropriate for the energy of a particular class of collisions. The power m comes from approximating the shielded Coulomb potential as a simple power law for incident particles of energy E and recoiling atoms of energy T. T is limited to the range 0 to $\gamma_{ij}E$ where γ_{ij} is the maximum fraction of the energy of the incident particle that can be transferred to the stationary atom: $\gamma_{ij} = 4M_iM_j/(M_i + M_j)^2$. The factor C_{ij} is calculated as:

$$C_{ij} = \frac{\pi}{2}\lambda_m a'_{ij}\left(\frac{M_i}{M_j}\right)^m (2A'_{ij})^{2m}, \quad m \leq 1/4, \tag{5.3}$$

where $a'_{ij} = 0.219\,\text{Å}$, $A'_{ij} \approx 52(Z_i Z_j)^{3/4}\,\text{eV}$, λ_m is a well defined constant dependent only on m, e the elementary charge, and $a_0 = 0.529\,\text{Å}$ the radius of the first Bohr orbital. The value of m often used on theoretical grounds is $m_{BM} = 0.055$, appropriate for a Born-Mayer potential. It is clear, as Sigmund has pointed out[27], that the factor γ_{ij} can only lead to preferential sputtering as a second order effect in the mass difference. This can most easily be seen[27] by writing

$$M_{i,j} = M \pm \delta M_{i,j}, \tag{5.4a}$$

where

$$\delta M_{i,j} \ll M, \tag{5.4b}$$

then $M^m_{i,j}$ becomes:

$$M^m_{i,j} = M^m \left(1 \pm m\frac{\delta M_{i,j}}{M} + \cdots\right), \tag{5.4}$$

and:

$$\gamma_{ij} = 1 - \left(\frac{\delta M_i - \delta M_j}{2M}\right)^2 \cdots \simeq 1. \tag{5.5}$$

The fact that the fractionation goes like $(M_i/M_j)^{2m}$ while C_{ij} only has a factor of $(M_i/M_j)^m$ can be traced[27] to two separate contributions to the fractionation according to Sigmund's theory. One factor of $(M_i/M_j)^m$ comes from the dependence in the nuclear stopping power S_j on C_{ij} and the other comes from a factor of C_{ij} in the cascade recoil density F_{ij}. Basically this means that lighter atoms are harder to stop (one factor) and easier to get going (the other factor).

If one assumes that $m = .055$ is a reasonable value then Sigmund's theory predicts an overall fractionation of 9.2‰ for the ^{92}Mo :^{100}Mo experiment. This is clearly low compared to the observed fractionation. The value of m, consistent with the theory, would be $m \approx 0.3$, typical of much higher energy collisions than are appropriate for use in sputtering theory. One objection to the application of this theory directly to the systems under consideration might be that if there is significant oxygen contamination at the surface of the Mo sample, then the average mass would be significantly lower than the average mass of the Mo isotopes. This

would be contrary to the condition of 5.4b. However, it should be noted that other experiments[10] seem to indicate that isotopic fractionation is relatively insensitive to the chemical composition of the sample in some cases, and Sigmund has readily compared predictions based on this theory to experiments[27] for which relation 5.4b is clearly not satisfied. In any case, the theory predicts no angular dependence on the isotopic fractionation and in most of the systems studied here there was clear angular dependence, even in the 'low fluence' limit.

5.2 Computer Simulations

There are several interesting advantages to using computer simulations to study isotopic fractionation in sputtering. The problem is 'reduced' to following the trajectories of atoms obeying some set of rules designed to approximate, to one degree or another, the actual trajectories of atoms in the cascade. There have developed two basic strategies for attacking this problem: The Binary Collision Approximation (BCA)[28], and Molecular Dynamics (MD)[29] simulation. The BCA approach is most appropriate in the high energy regime where collisions occur with distances of closest approach that are small compared to the average distance between atoms. As the energy falls, special 'tricks' need to be employed to keep track of weak, simultaneous collisions. The advantage of such a scheme is simplicity and speed. Because atoms are assumed to be stationary until involved in a collision there is no need to keep track of any atoms other than those in the cascade (i.e., with enough energy to be sputtered). Collisions are dealt with using approximate scattering integrals treated as two body events. There is essentially no limit to the depth scale that can be included in the cascade, and the number of atoms involved can become quite high without seriously degrading performance. The MD version is comparatively slow and (currently) limited in its ability to deal with large targets and deep cascades. But its superior performance at low energy makes it an ideal approach for sputtering calculations where, presumably, the low energy regime is most important. The idea is to follow the motion of every atom in the target by integrating Newton's Second Law assuming some interaction potential between the atoms.

This potential can become quite sophisticated, including, for example, many body effects[23] and periodic boundary conditions. The results of the experiments carried out here compare favorably with the results of MD simulations, which indicate both larger fractionations than predicted by equation 5.1, and angular dependence of the isotopic fractionation[23] that is excluded by the analytical theory altogether[27].

A monte carlo BCA code has been developed to simulate, at least qualitatively, the systems discussed here so that some more insight might be gained as to the nature of the physical processes that lead to fractionation and to the cause of the apparent failure of the analytical theory in explaining them. At this time the effort is only beginning but it has shown some interesting results. The following is a basic description of the code, which closely resembles the TRIM and TRIDYN programs[28,30,31] used for many radiation damage, preferential sputtering, and ion implantation studies. The latest results are discussed in relation to the analytical theory, experimental results, and results from MD simulations.

The strategy used here was to follow a series of randomly selected binary collision partners until the energy of any atom dropped below the surface binding energy, therefore making no further contribution to the sputtering yield, or the atom was sputtered. A 'collision' consisted of the following sequence of events:

1) For the current atom under study its direction was picked as the local z' axis. A distance λ from its current position a plane was erected perpendicular to the direction of motion. From a circular area $A = \pi b_{max}^2$ on this plane the coordinates of the collision partner were selected from a uniform distribution. The identity of the partner was determined from the local isotopic and chemical composition of the target, which was allowed to vary with depth below the surface. The mean free path λ and the maximum impact parameter b_{max} were chosen so that $A\lambda = 1/n$, where n was the local average atomic density of the target. Usually $\lambda \sim n^{-1/3}$.

2) If the partner atom, so picked, existed (i.e., was located within the volume of the target) the collision integral was evaluated using the 'Magic Formula' of

TRIM[28]. This is essentially a parameterized fit for the scattering angle θ as a function of reduced energy and impact parameter, appropriate for approximate interaction potentials between atoms in a solid. The result of the calculation gives, as a 'bonus,' the distance of closest approach between the two atoms involved in the collision. This could optionally be used in the calculation as part of the electronic stopping of recoil atoms according to the formalism of Oen and Robinson[32]. Also before the collision, one could optionally add an electronic loss proportional to the length of the path and $\sqrt{E}$.

3) Once the scattering calculation was complete the atoms' new directions were set, assuming the partner started at rest in the target. The scattering directions were determined first in the local basis of the incoming atom, and then converted to the coordinate system of the target. The incoming atom was then propagated to its new location in the target. The distance of propagation was the mean free path λ minus the so called *time integral* τ, which is simply a correction for the fact that, after the collision, the incoming atom appears to come from a point somewhat before the plane of the partner.
4) Finally the partner atom was followed until it, and all its partner atoms, were sputtered or stopped, and then the steps were repeated for the incoming atom. This highly recursive algorithm was implemented as a single recursive function in the 'C' programming language insuring that all collisions were treated equivalently.

The target composition can also be adjusted and 'relaxed' in response to the bombardment by keeping track of the number of atoms originating and stopping in discrete layers of the target. As the composition profile of the target changes the sputtering yield naturally responds, ultimately leading to a steady state profile.

Some results of the simulation are plotted in figure 5.1, which shows the ratio of ^{92}Mo to ^{100}Mo atoms sputtered into angular bins from 0–30°, 30–60°, and 60–90°. The 'target' in this case was 90% Mo (50:50 mixture of isotopes) and 10% Oxygen to try to account for an oxidized layer. It is difficult to make any

clear interpretation of these results at this early stage, due to the poor statistics accumulated so far; however, it does appear that although overall sputtering yield of Mo calculated in this case is about right ($Y \sim 3$), the isotopic fractionation is much more nearly consistent with the analytical theory than the experiment. The oxygen, on the other hand is clearly sputtered very preferentially compared to the Mo, as would be expected due to its much smaller mass. It seems that the failing of the analytical theory cannot be explained by simply saying that it treats the surface or the time evolution of the cascade too naively. The Monte Carlo BCA strategy, while admittedly somewhat simplistic, allows for considerable complexity in the cascade, including anisotropic momentum distributions, essentially arbitrary energy distributions, sophisticated treatment of electronic stopping, and a realistic treatment of an atomically 'rough' surface. Yet it also appears to fail to predict the measured fractionation, at least in the relatively simple form used here.[5.1] This may indicate that the essential ingredient missing from the analytical theory and the BCA strategy, both of which perform well when predicting the *total* sputtering yield, is the ability to deal with low-energy many-body collisions, which allows the MD approach to match more nearly the experimental result. There is also evidence that even within the MD simulation arena one can find significant differences between calculations done with two-body potentials and many body-potentials[23]. These kinds of subtleties would be very difficult to incorporate into either a BCA or an analytical approach.

5.3 Outlook and Summary of Results

Significant advances have been made in the experimental determination of the angular dependence and the overall size of isotopic fractionation due to sputtering

[5.1] There are several improvements[30] one might make to the basic MCBCA scheme. These include allowing for multiple, simultaneous, weak collisions under some circumstances where a significant fraction of the energy of an atom can be lost in large impact parameter collisions, and a more sophisticated treatment of the surface. It is not yet clear whether addition of these improvements would significantly alter the results.

under keV ion bombardment, especially in the low fluence regime, using a simple collection technique and SIMS analysis. The effects are larger than is predicted by the dominant analytical theory and are similar to the results of some MD computer simulations[23]. There is a rather striking angular variation in the fractionation, most clearly seen in the 5keV Xe^+ on Mo data that indicates a 3% drop in δ_{ij} from the near normal to the oblique direction.

Isotopic fractionation has also been studied in the liquid metal In:Ga eutectic and suggests that something very interesting is happening in the inhomogeneous surface layer where the In concentration goes from the bulk value of $\sim$ 10% to the enriched value of $\sim$ 97%. Whereas the fractionation of the In isotopes falls with angle, in a fashion similar to the Mo isotopes from the solid target experiments, the Ga fractionation goes *up* with angle indicating a different mechanism most likely associated with the In-rich layer at the surface.

The In:Ga experiments suggest some possibly interesting future investigations. The advantages of using a liquid target for studying isotopic fractionation are numerous, as presented in chapter 4. There are however several problems with the In:Ga system that would be avoided in an experiment using pure Ga metal. One could imagine sputter cleaning the target in the liquid state, effectively removing any surface contaminants. Then the target could be re-frozen and sputtered, in solid form, until a steady state flux is achieved. Frozen In:Ga eutectic measurements would be difficult to interpret due to the presence of the In enriched surface layer. Interpretation of frozen Ga data would presumably be straightfoward. The frozen Ga system could be measured to get an R_{ij}^{STD} reference for an *absolute* isotopic fractionation measurement as a function of dose. The beauty of this is that to run a 'new' sample, one merely needs to melt the target and re-freeze! Naturally the measurement could also be done in the liquid state to get *zero fluence* data.

The use of a Monte Carlo Binary Collision Approximation (MCBCA) calculation to describe isotopic fractionation is being investigated. The latest results indicate that this technique produces fractionation values much more nearly in

agreement with the analytical theory than with the experimental data. It is suggested that this might help determine the essential physics required to describe mass fractionation properly. Important things seem to be happening in the low-energy many body regime, where the Molecular Dynamics approach is more appropriate and appears to produce results more nearly in agreement with the experimental data.

Appendix A

Factors Involved in Maintaining a Clean Surface

During a sputtering experiment the target surface is exposed to bombardment by an ion beam that has been carefully energy and momentum analyzed so that its properties are well understood. Unfortunately it is also exposed to a flux of unwanted particles that constitute the residual gas inside the target chamber. In the best of all possible worlds the background pressure in the target chamber due to the residual gas would be zero. The purpose of the following discussion is to point out the necessary conditions on the vacuum system, ion beam current, and timescale of the experiment required to maintain a 'clean' surface during the course of a sputtering experiment.

According to the classical equipartition theorem, atoms and molecules in an ideal gas each get $\frac{1}{2}kT$ of translational kinetic energy per degree of freedom. The implication being that $v_{\rm rms}$ for atoms at a temperature T is $\sqrt{3kT/m}$. This results in a flux of particles ϕ per unit area per unit time striking an arbitrary surface[33]:

$$\phi = \frac{P}{\sqrt{2\pi mkT}}, \qquad (A.1)$$

where P is the pressure, T is the temperature, m is the particle mass and k is Boltzmann's constant. If a fraction f of the particles striking the surface actually stick to it, then the rate of sticking will be $f\phi$. In order for the surface to remain clean, the rate at which atoms are sputtered must exceed, by some considerable margin, the rate at which new residual atoms stick to the surface. If the total sputtering yield is Y and the incident ion beam flux is I incident ions per unit area per unit time, then the condition becomes:

$$f\phi \ll YI. \qquad (A.2)$$

The effort to reduce the product $f\phi$ has been centered on reducing ϕ by keeping the pressure of residual gasses in the target chamber as low as possible. Typical base

pressures in the target chamber, before an experiment, were in the neighborhood of 10^{-9} Torr. The target chamber pressure invariably rose with the addition of beam, but this additional pressure was likely dominated by the ion source gas, and hence made little contribution to the effective $f\phi$ since, presumably, f is small for noble gasses that are only weakly adsorbed to most surfaces. Additionally f was kept as small as possible by raising the temperature of the target to 150 C° during the bombardment, which should have removed any weakly adsorbed atoms from the surface.

In order to reach such pressures, several additional precautions had to be taken. All components to be loaded into the target chamber were cleaned and/or etched carefully beforehand. All parts were rinsed in an ultrasonic bath of reagent grade isopropyl alcohol and warm air dried before being introduced into the UHV environment. Cleaned parts were handled only with clean tools and gloved hands. Only UHV compatible materials could be used in the construction of the apparatus. This included type 304 stainless steel structural supports, OFHC or 99.995% pure copper conductors, MACOR or alumina insulators and carefully cleaned Ta collimators. After the fully assembled apparatus was loaded into the target chamber, it was evaluated to 10^{-6} Torr and then the entire chamber was baked at 300 C° for at least 24 hours until the base pressure reached 10^{-9} Torr when cool. At this base pressure, with the beam current densities used in these studies, relation A.2 could be easily satisfied.

Appendix B

Calculation of the Ratio of Two Isotopes From SIMS Data

Several different approaches to analyzing the SIMS data were investigated as a part of this study. It was discovered that there are some subtleties associated with taking the ratio of two quantities that are known with finite precision. This appendix briefly describes the nature of these subtleties and the methods used here to avoid the associated pitfalls.

Data was taken from the Caltech PANURGE ion probe (a modified Cameca IMS-3f)[15] as a function of time. The computer cycled the magnet from one peak to another and counted the number of secondary ions from each peak for the same length of time (typically 2 to 10 seconds.) The result was a sequence of ion counts for a set of different times for each peak under investigation. Because the count rate was roughly proportional to the coverage of sputtered atoms on the collector surface the count rate generally fell as a function of time. A typical set of data can be found in figure B.1. This data was taken from the Mo experiment, 5 keV Xe^+ at a fluence of 0.3×10^{15} cm^{-2}.

One problem was that data for different isotopes was taken at different times, while the coverage of atoms on the collectors was changing as a function of time and thereby changing the count rate for both isotopes. In order to correct for this effect the data for one isotope was interpolated between two measurements to a get an 'averaged' value appropriate for the intermediate time during which the other isotope was measured. It was this interpolated count that was used to get an isotope ratio for that intermediate time. Then the ratios calculated for each cycle were combined in a weighted average for the entire run, the weights being determined by the statistical uncertainties of the individual ratios. This averaged ratio was then used to determine the relative isotope ratio for that run by comparing it to R_{ij}^{STD}.

Unfortunately it appears that there is an additional built-in bias to the above procedure that was not immediately recognized. If, at some time during a run, a number of ions is measured, it is only 'measured' in a statistical sense (i.e., it is effectively drawn from a distribution of counts that has a well defined set of statistical moments). Let's say that the expectation value of counts from the light isotope is $\mu_A = \langle A \rangle$ and the corresponding value from the heavy isotope is $\mu_B = \langle B \rangle$. What we *wish* to measure is $\mu_A/\mu_B = \langle A \rangle / \langle B \rangle$. What we get when we average in the above sense is more nearly

$$\mu_{A/B} = \langle A/B \rangle. \qquad (B.1)$$

That these two quantities are different is the main point of this appendix.

In order to study this effect a more sophisticated approach was taken. A monte carlo, non-linear least squares program was written that fit the data in a non-biased fashion (i.e., both isotopes were treated in an entirely equivalent manner). The ratio of isotopes was one parameter and the coverage as a function of dose was fit using a linear superposition of Legendre Polynomials and a non-linear exponential multiplier, both of which were functions of time. The result was a non-biased estimator of the isotope ratio. Because this program was written using monte-carlo error estimation it was easily modified to produce 'pseudo-data' representing well known isotope ratios that could be analyzed with any technique to see built-in biases directly. This program was then used to test other calculations.

The simplest alternative to the 'running average' calculation was the 'sum then average' technique. In other words, add the counts from a single isotope for an entire run taking into account appropriate weighting at the endpoints, then calculate the ratio of the sums afterwards. At first glance this may seem equivalent to the original scheme, but it is not. By summing the counts from one isotope for an entire run the relative statistical uncertainty is reduced significantly $\sim 1/\sqrt{N}$. This means that non-linear fluctuations in the denominator do not bias the results away from the 'true' mean as badly.

The net result of the pseudo-data tests was that, for the typical count rates

found in the lowest coverage runs used in these investigations, the results of the running average technique were biased by about 1σ from the 'true mean' (i.e., the ratio used by the computer to generate the pseudo-data). The sum then average technique, and the non-linear least squares techniques, on the other hand gave consistent results, within statistical uncertainty, equally distributed above and below the 'true mean.' Table B.1 gives example results for the data shown in figure B.1.

Table B.1 Example of differences between three computational techniques used to determine the raw isotope ratio for the SIMS studies.

Technique	Ratio[a]
Running Average with Interpolation	$1.172 \pm .012$
Sum then Average	$1.177 \pm .012$
Nonlinear Least Squares with M.C. Error Estimation	$1.178 + .012 - .013$[b]

a. Errors shown are $\pm 2\sigma$.

b. The Monte Carlo error is a 95% confidence interval.

There may be better estimators than the non-linear least squares code or the sum then average techniques used here, but because they give reasonable results when applied to the computer generated pseudo-data, they were considered sufficient for these studies. The sum then average result never differed significantly from the more sophisticated non-linear least squares calculation and so was used throughout the study because it was much faster.

References

[1] W. R. Grove, Philos. Mag. **5** (1853) 203.

[2] T. A. Tombrello, Rad. Effects **65** (1982) 389.

[3] L. C. Feldman and J. W. Mayer, *Fundamentals of Surface and Thin Film Analysis* (North-Holland, New York, 1986).

[4] H. L. Garvin, E. Garmire, S. Somekh, H. Stoll and A. Yariv, Appl. Optics **12** (1973) 455.

[5] P. Sigmund in *Sputtering by Particle Bombardment* I, R. Behrisch, ed., Topics Appl. Phys., Vol. 47 (Springer, Berlin, Heidelberg, New York, 1981).

[6] M. W. Thompson, Physics Reports, 69, **4**, (1981), 335.

[7] H. Gnaser, H. Oechster, submitted to Nucl. Instr. Meth. B (1989).

[8] H. Gnaser, H. Oechster, Phys. Rev. Lett. 63 **24** (1989) 2673.

[9] J. M. Fluit, L. Friedman, A. J. H. Boerboom and J. Kistemaker, J. Chem. Phys. **35** (1961) 1143.

[10] W. A. Russell, D. A. Papanastassiou and T. A. Tombrello, Rad. Effects **52** (1980) 41.

[11] O. Arai, Y. Tazawa, T. Shimamura and K. Kobayashi, Jpn. J. Appl. Phys. **18** (1979) 1231.

[12] N. Shimizu and S. R. Hart, J. Appl. Phys. **53** (1982) 1303.

[13] H. Gnaser and I. D. Hutcheon, Surface Sci. **195** (1988) 499.

[14] L. M. Baumel, M. R. Weller, R. A. Weller and T. A. Tombrello, Nucl. Instr. Meth. **B34** (1988) 427.

[15] J. C. Huneke, J. T. Armstrong and G. J. Wasserberg, Geochim. Cosmochim. Acta **47** (1983) 1635.

[16] H. Gnaser and I. D. Hutcheon, Phys. Rev. **B35** (1987) 877.

[17] S. A. Schwarz, J. Vac. Sci. Technol. **A5** (1987) 308.

[18] H. Gnaser and I. D. Hutcheon, Phys. Rev. **B38** (1988) 11112.

[19] N. D. Lang, J. K. Novskov, Physica Scripta, **T6** (1983).

[20] D. L. Weathers, Thesis, California Institute of Technology, May 1989.

[21] M. H. Shapiro and T. A. Tombrello, Nucl. Instr. Meth. **B18** (1987) 355.

[22] M. Shapiro, T. Tombrello, D. E. Harrison, Nucl. Instr. Meth. **B30** (1988) 152.

[23] D. Lo, et al., J. Vac. Sci. Tech A**6** (1988) 718.

[24] M. Dumke, Thesis, California Institute of Technology, (1983).

[25] K. Hubbard, Thesis, Yale University, (1988).

[26] P. Sigmund, Phys. Rev. **184** (1969) 383.

[27] P. Sigmund, Nucl. Instr. Meth. B**18** (1987) 375.

[28] J. P. Biersack, Nucl. Instr. Meth. B**27** (1987) 21.

[29] M. M. Jakas and D. E. Harrison Jr., Nucl. Instr. Meth. B**14** (1986) 535.

[30] J. Biersack, W. Eckstien, Appl. Phys. A**34** (1989) 73.

[31] W. Moller, W. Eckstien, Nucl. Instr. Meth. B**2** (1984) 814.

[32] O. Oen, M. Robinson, Nucl. Instr. Meth. **132** (1976) 647.

[33] T. L. Hill, *An Introduction to Statistical Thermodynamics* (Addison-Wesley, Reading, MA, 1960).

Figure Captions

Figure 2.1 Ion Optics for the Mo experiments
Schematic layout of the keV ion accelerator used in the Mo experiments showing (a) the ion beam optics, and (b) the collimation and electron supression scheme. The beamline entering on the left is the Mev line from the 6MV Tandem Van De Graaff accelerator.

Figure 2.2 The sputtering apparatus for the Mo experiments
Perspective diagram of the collimator and collector assemblies. The collectors are shown pulled away from the target block for clarity. The target block was as shown except that there were three fin/target combinations to allow different experiments without venting the chamber.

Figure 3.1 $^{92}Mo/^{100}Mo$ vs. ion beam fluence
Fractionation of Mo isotopes as a function of accumulated ion beam fluence (a) Ar^+ and (b) Xe^+ bombardment. The error bars are $\pm 2\sigma$.

Figure 3.2 $^{92}Mo/^{100}Mo$ vs. angle for 5 keV Xe^+
Fractionation of Mo isotopes under 5 keV Xe^+ bombardment as a function of angle with doses of (a)0.3×10^{15} ions/cm^2 and (b)0.61×10^{15} ions/cm^2. The error bars are $\pm 2\sigma$.

Figure 3.3 $^{92}Mo/^{100}Mo$ vs. angle for 5 keV Xe^+
Fractionation of Mo isotopes under 5 keV Xe^+ bombardment as a function of angle with doses of (a)1.0×10^{15} ions/cm^2 and (b)1.82×10^{15} ions/cm^2. The error bars are $\pm 2\sigma$.

Figure 3.4 $^{92}Mo/^{100}Mo$ vs. angle for 5 keV Xe^+
Fractionation of Mo isotopes under 5 keV Xe^+ bombardment as a function of angle with doses of (a)4.29×10^{15} ions/cm^2 and (b)7.93×10^{15} ions/cm^2. The error bars are $\pm 2\sigma$.

Figure 3.5 $^{92}Mo/^{100}Mo$ vs. angle for 5 keV Xe^+
Fractionation of Mo isotopes under 5 keV Xe^+ bombardment as a function of angle with a dose of 20.05×10^{15} ions/cm^2. The error bars are $\pm 2\sigma$.

Figure 3.6 $^{92}Mo/^{100}Mo$ vs. angle for 10 keV Xe^+
Fractionation of Mo isotopes under 10 keV Xe^+ bombardment as a function of angle with doses of (a)0.61×10^{15} ions/cm^2 and (b)9.74×10^{15} ions/cm^2. The error bars are $\pm 2\sigma$.

Figure 3.7 $^{92}Mo/^{100}Mo$ vs. angle for 5 keV Ar^+
Fractionation of Mo isotopes under 5 keV Ar^+ bombardment as a function of angle with doses of (a)1.22×10^{15} ions/cm^2 and (b)20.63×10^{15} ions/cm^2. The error bars are $\pm 2\sigma$.

Figure 3.8 $^{92}Mo/^{100}Mo$ vs. angle for 10 keV Ar^+
Fractionation of Mo isotopes under 10 keV Ar^+ bombardment as a function of angle with doses of (a)1.21×10^{15} ions/cm^2 and (b)19.45×10^{15} ions/cm^2. The error bars are $\pm 2\sigma$.

Figure 4.1 In and Ga fractionation vs. angle
Fractionation of (a) In and (b) Ga isotopes under 20 keV Ar^+ bombardment as a function of angle. The error bars are $\pm 2\sigma$.

Figure 5.1 MCBCA simulation results
The simulated sputtered fractionation of (a) Mo isotopes (i.e., $^{92}Mo/^{100}Mo$) and the sputtered fraction of (b) O atoms (i.e., O/Mo) as a function of angle at zero simulated fluence.

Figure B.1 Raw SIMS data from the Mo experiment
Raw isotope counts for an example SIMS run. This particular set of data was taken from the 5.0 keV Xe^+ bombardment with the lowest dose (i.e., 0.3×10^{15} ions/cm^2).

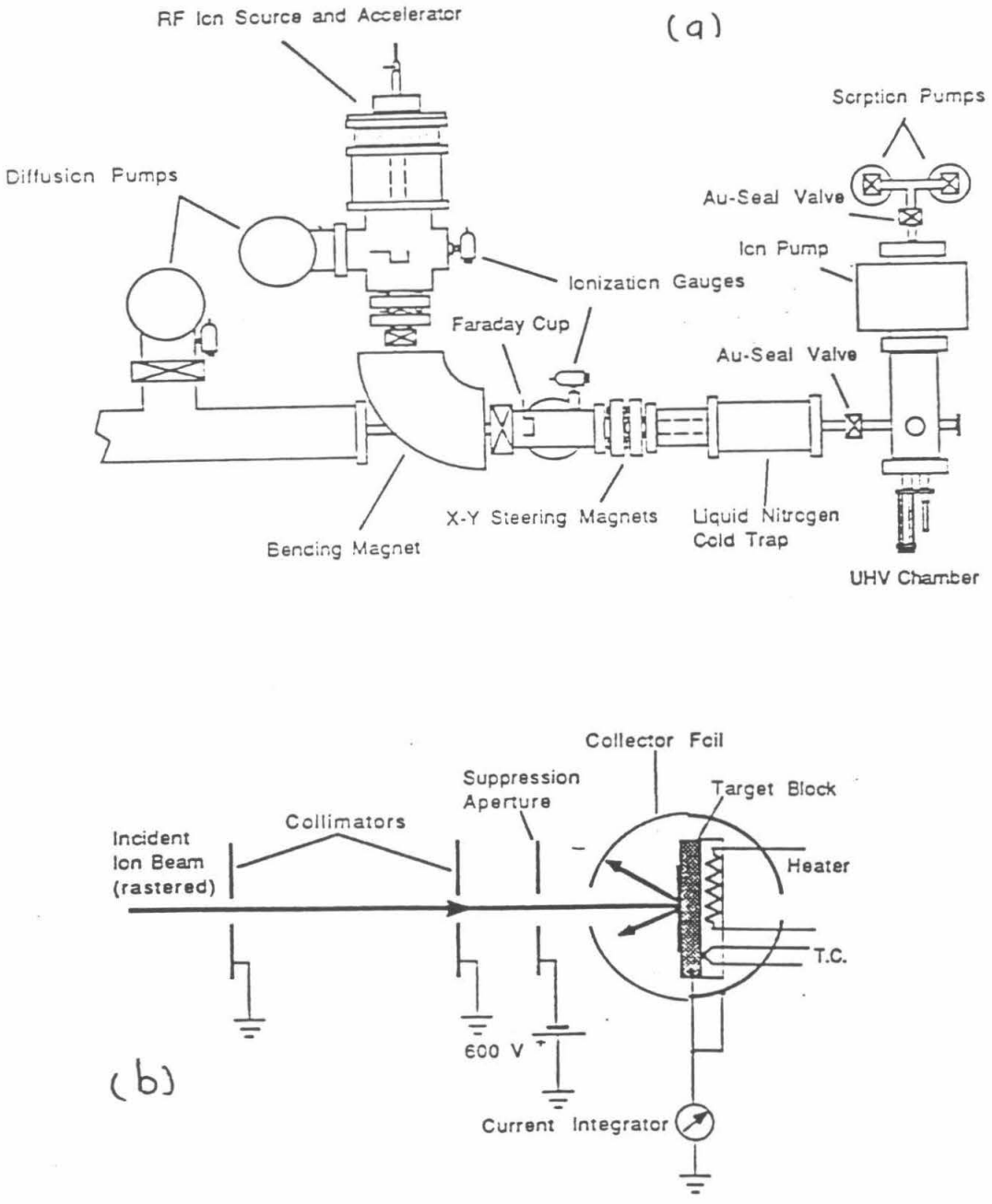
RF Ion Source and Accelerator
(a)
Sorption Pumps
Diffusion Pumps
Au-Seal Valve
Ion Pump
Ionization Gauges
Faraday Cup
Au-Seal Valve
X-Y Steering Magnets
Liquid Nitrogen
Cold Trap
Bending Magnet
UHV Chamber
Collector Foil
Suppression
Aperture
Target Block
Collimators
Incident
Ion Beam
(rastered)
Heater
T.C.
600 V
(b)
Current Integrator

Figure 2.1

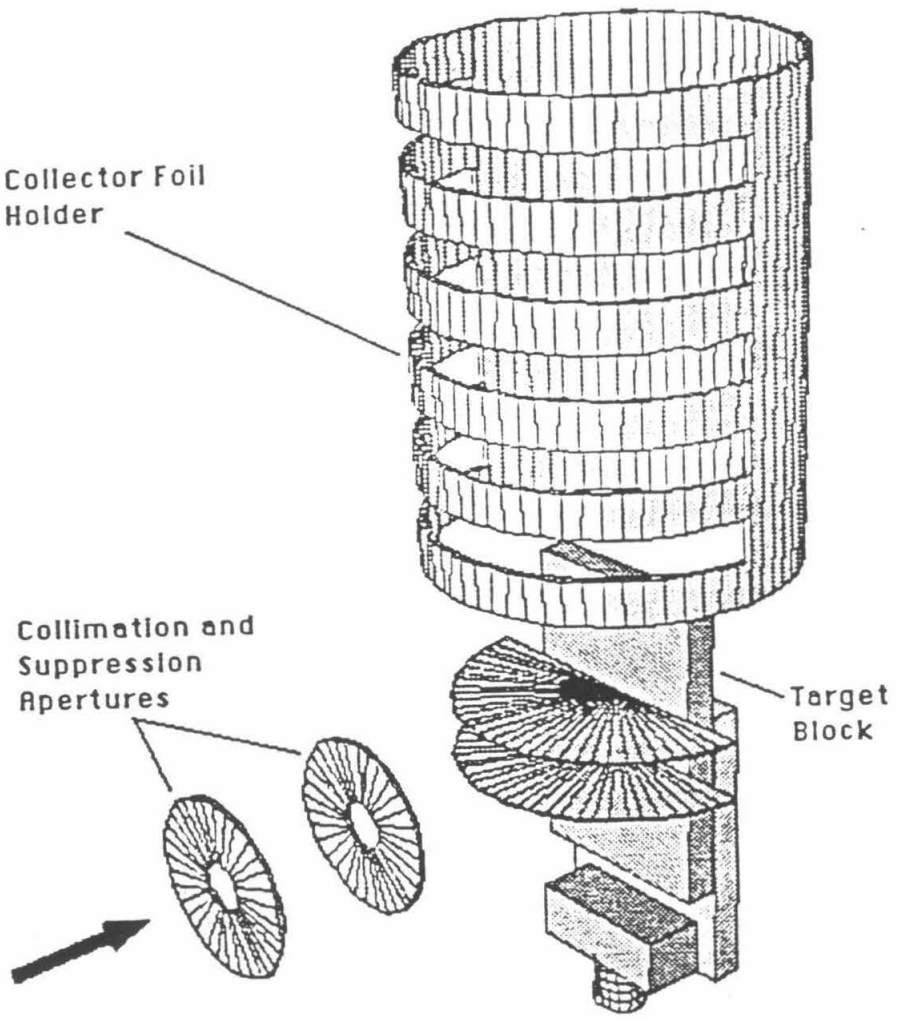
Collector Foil
Holder
Collimation and
Suppression
Apertures
Target
Block

Figure 2.2

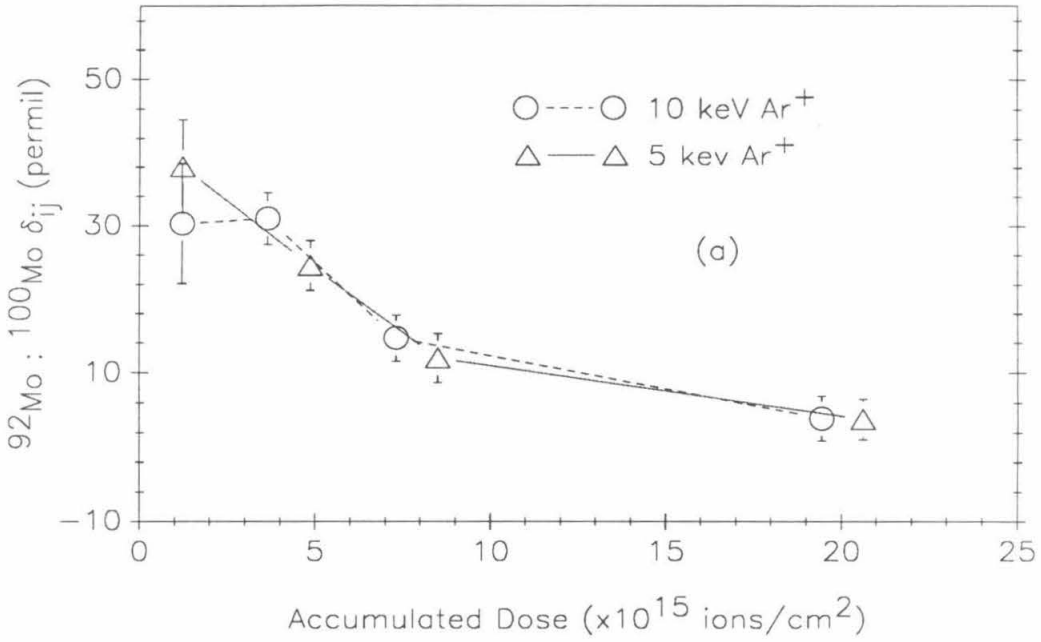
50
30
10
−10
0
5
10
15
20
25
O---O 10 keV Ar+
Δ—Δ 5 kev Ar+
(a)
92Mo : 100Mo δij (permil)
Accumulated Dose (x10^15 ions/cm^2)

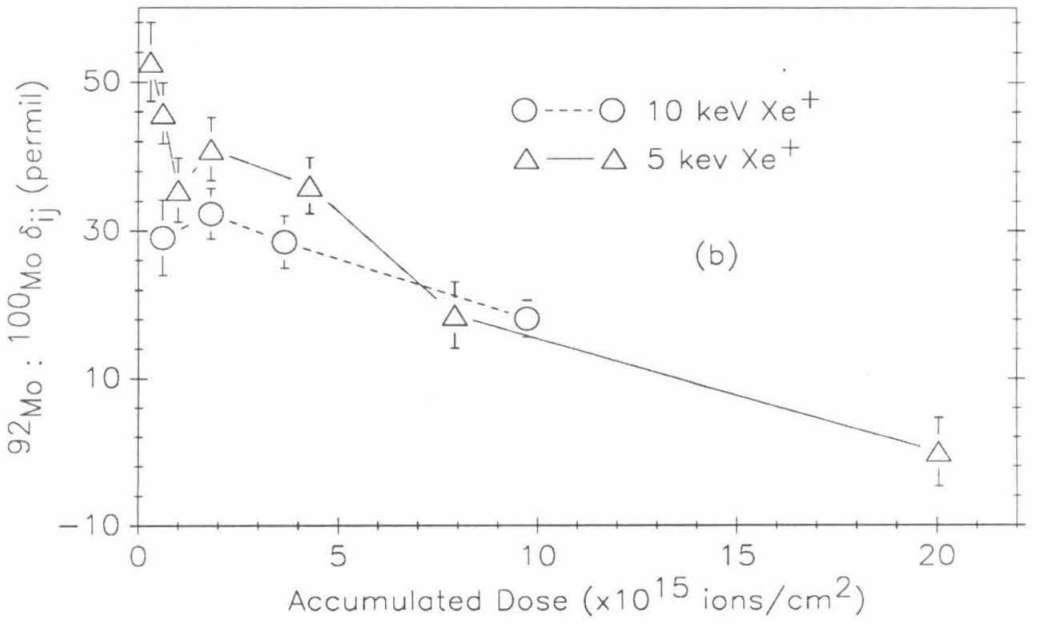
50
30
10
−10
0
5
10
15
20
O---O 10 keV Xe+
Δ—Δ 5 kev Xe+
(b)
92Mo : 100Mo δij (permil)
Accumulated Dose (x10^15 ions/cm^2)

Figure 3.1

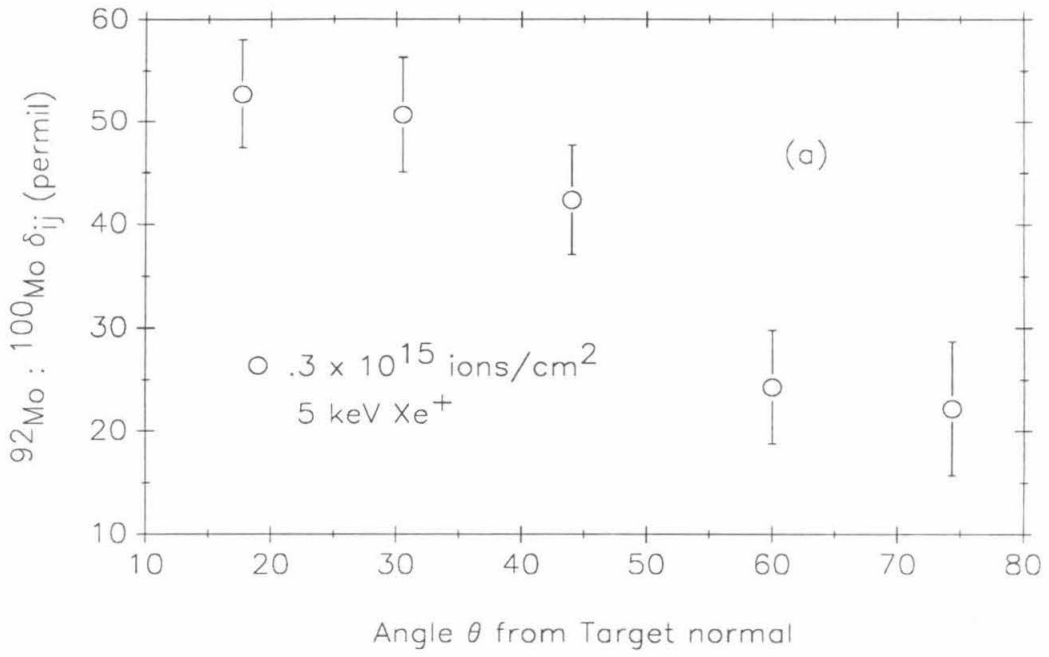
60
50
40
30
20
10
10
20
30
40
50
60
70
80
(a)
○ .3 x 10^15 ions/cm^2
5 keV Xe+
92Mo : 100Mo δij (permil)
Angle θ from Target normal

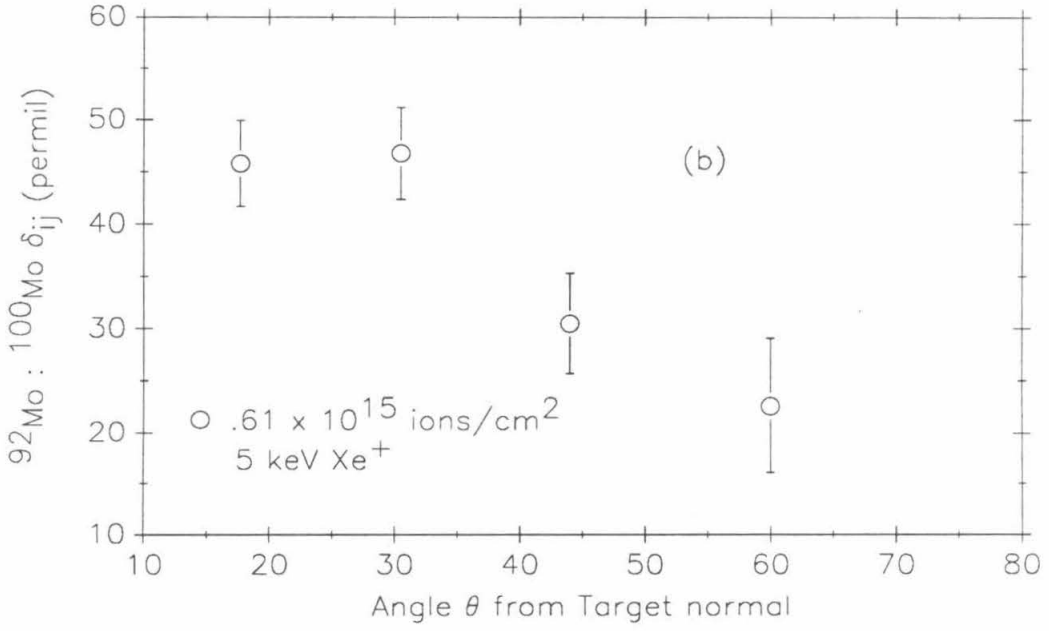
60
50
40
30
20
10
10
20
30
40
50
60
70
80
(b)
○ .61 x 10^15 ions/cm^2
5 keV Xe+
92Mo : 100Mo δij (permil)
Angle θ from Target normal

Figure 3.2

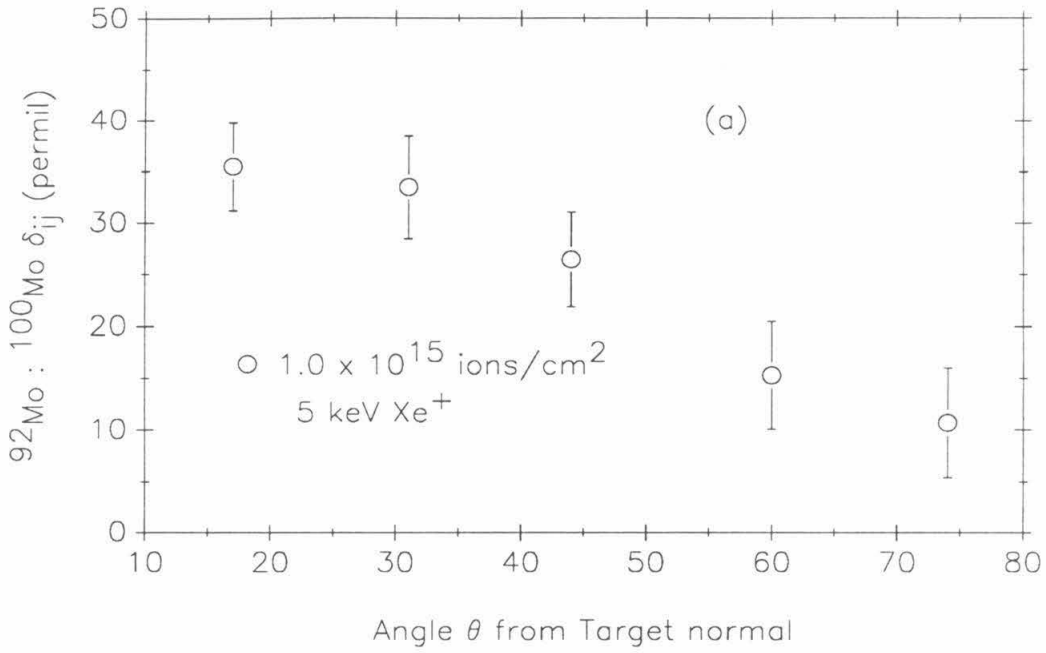
50
40
30
20
10
0
10
20
30
40
50
60
70
80
(a)
○ 1.0 x 10^15 ions/cm^2
5 keV Xe+
92Mo : 100Mo δij (permil)
Angle θ from Target normal

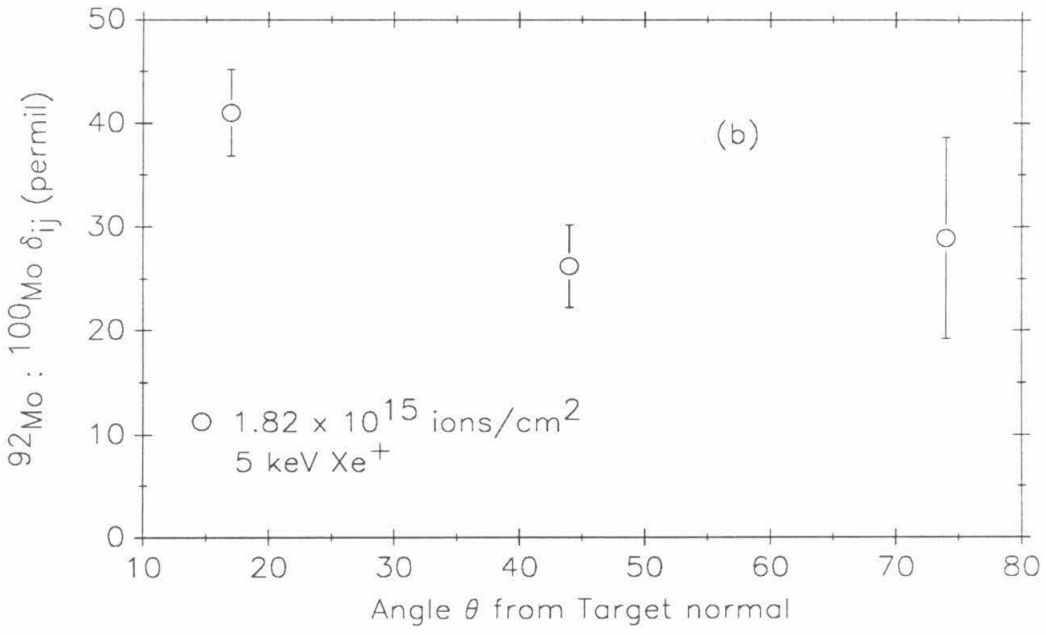
50
40
30
20
10
0
10
20
30
40
50
60
70
80
(b)
○ 1.82 x 10^15 ions/cm^2
5 keV Xe+
92Mo : 100Mo δij (permil)
Angle θ from Target normal

Figure 3.3

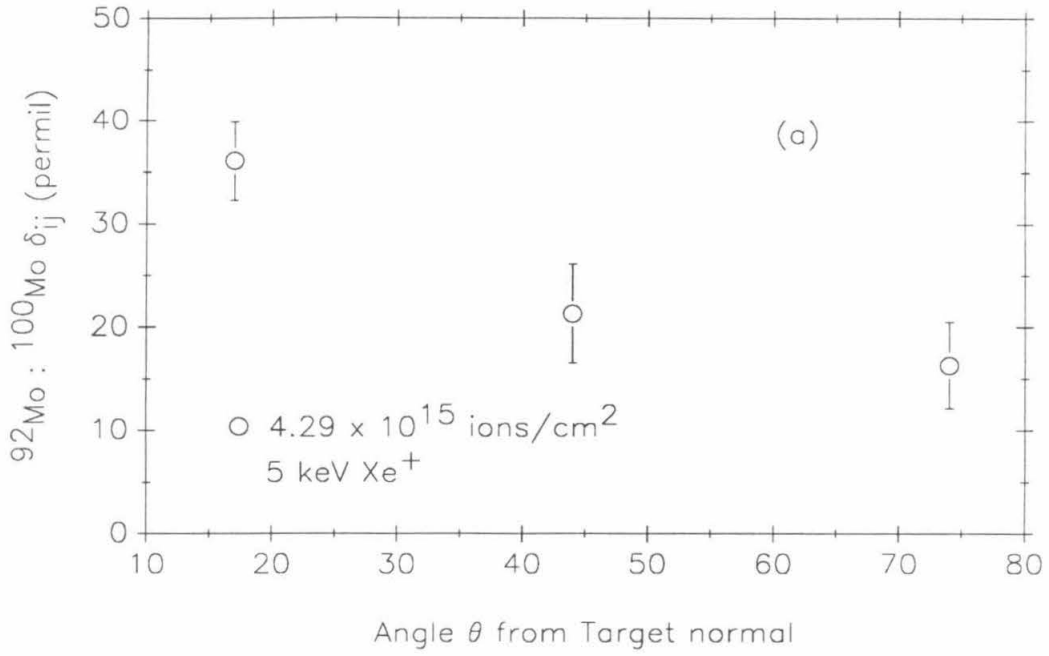
50
40
30
20
10
0
10
20
30
40
50
60
70
80
(a)
O 4.29 x 10^15 ions/cm^2
5 keV Xe+
92Mo : 100Mo δij (permil)
Angle θ from Target normal

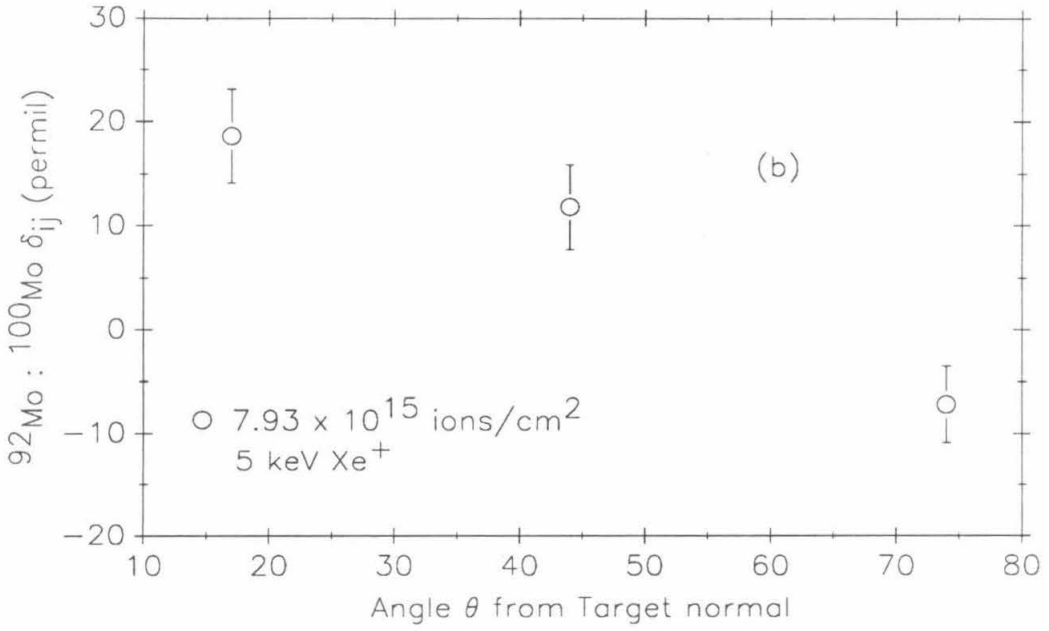
30
20
10
0
−10
−20
10
20
30
40
50
60
70
80
(b)
O 7.93 x 10^15 ions/cm^2
5 keV Xe+
92Mo : 100Mo δij (permil)
Angle θ from Target normal

Figure 3.4

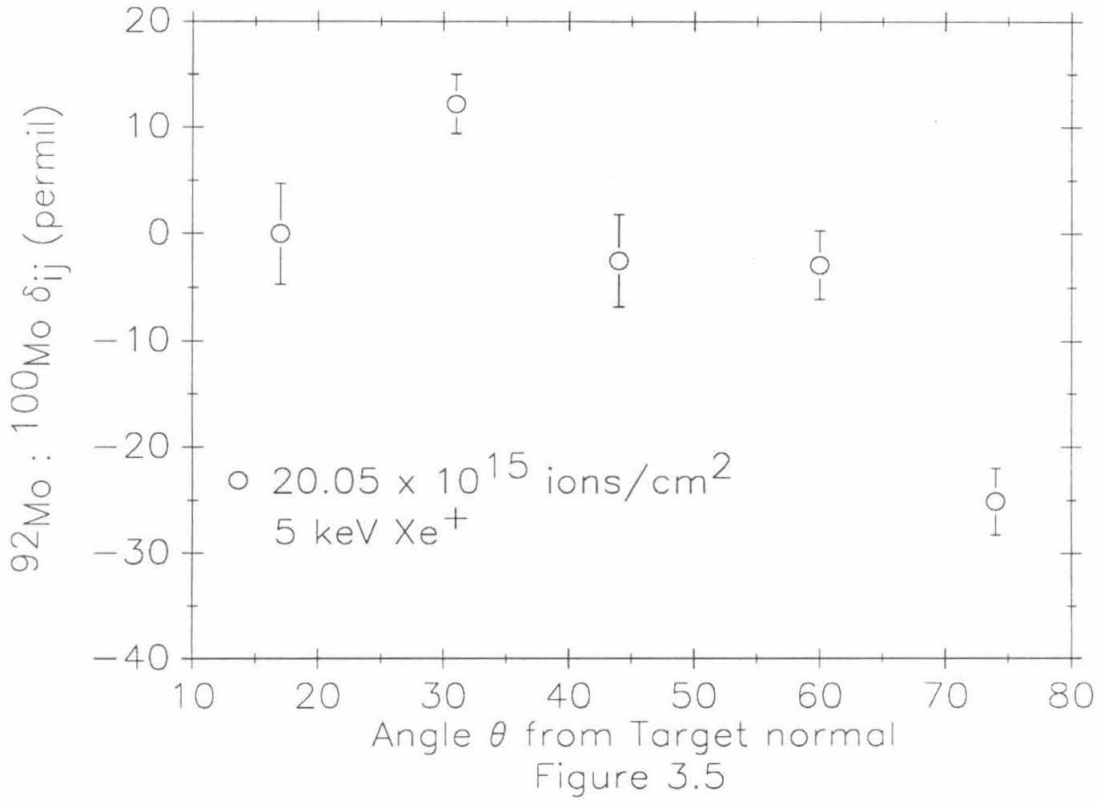
20
10
0
−10
−20
−30
−40
10
20
30
40
50
60
70
80
$^{92}Mo : {}^{100}Mo\ \delta_{ij}$ (permil)
o 20.05 x 10^{15} ions/cm^2
5 keV Xe^+
Angle θ from Target normal

Figure 3.5

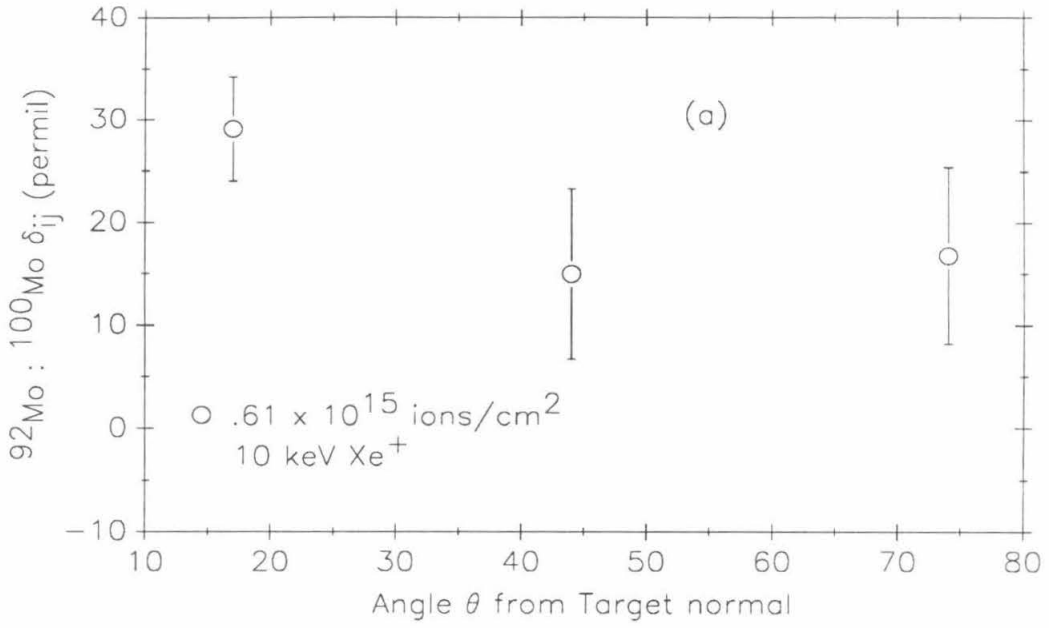
40
30
20
10
0
−10
(a)
$92_{Mo} : 100_{Mo}\ \delta_{ij}$ (permil)
○ .61 x 10^{15} ions/cm^2
10 keV Xe^+
10
20
30
40
50
60
70
80
Angle θ from Target normal

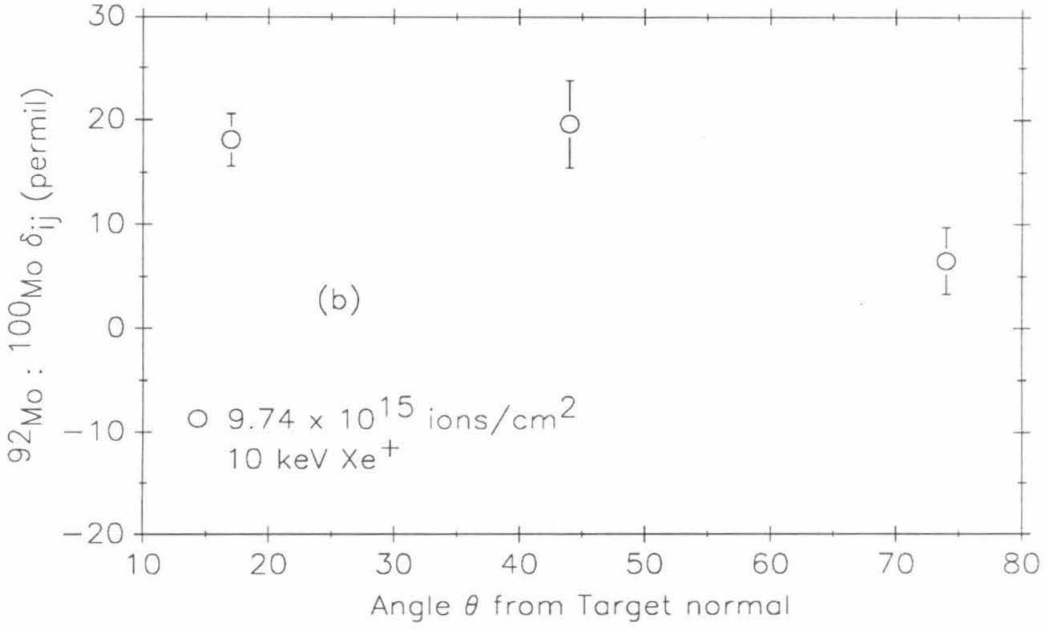
30
20
10
0
−10
−20
(b)
$92_{Mo} : 100_{Mo}\ \delta_{ij}$ (permil)
○ 9.74 x 10^{15} ions/cm^2
10 keV Xe^+
10
20
30
40
50
60
70
80
Angle θ from Target normal

Figure 3.6

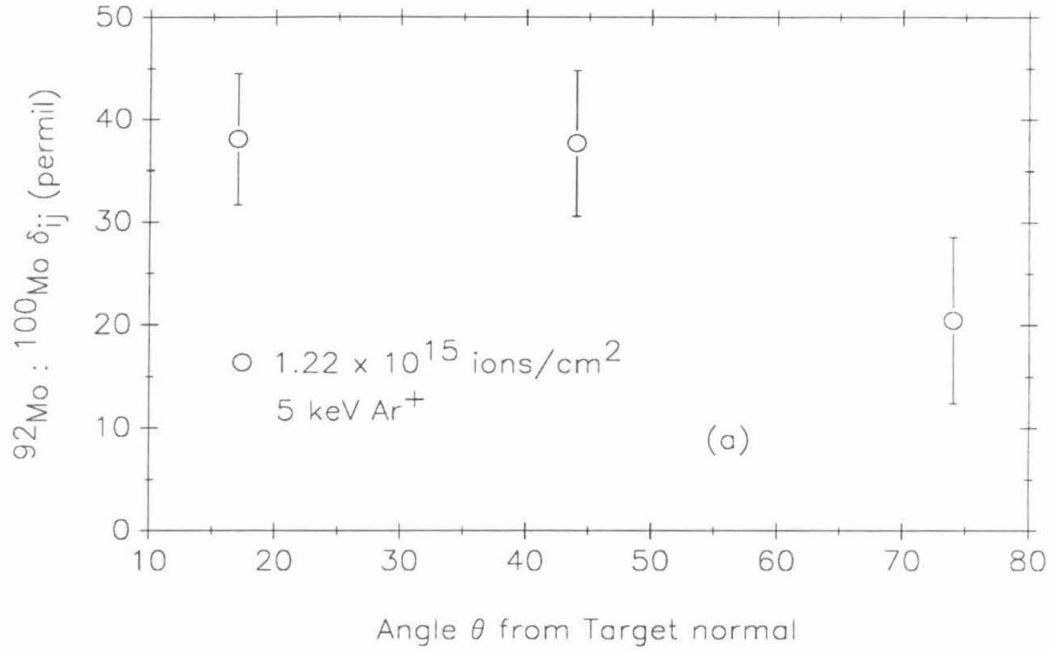
50
40
30
20
10
0
10
20
30
40
50
60
70
80
^{92}Mo : ^{100}Mo δ_{ij} (permil)
○ 1.22 x 10^{15} ions/cm^2
5 keV Ar$^+$
(a)
Angle θ from Target normal

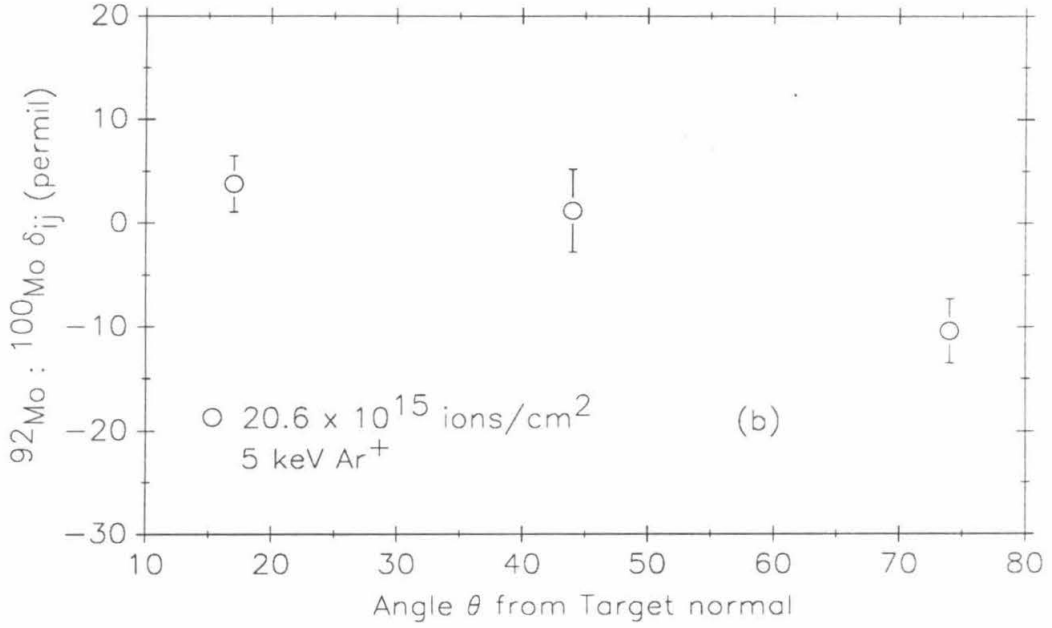
20
10
0
−10
−20
−30
10
20
30
40
50
60
70
80
^{92}Mo : ^{100}Mo δ_{ij} (permil)
○ 20.6 x 10^{15} ions/cm^2
5 keV Ar$^+$
(b)
Angle θ from Target normal

Figure 3.7

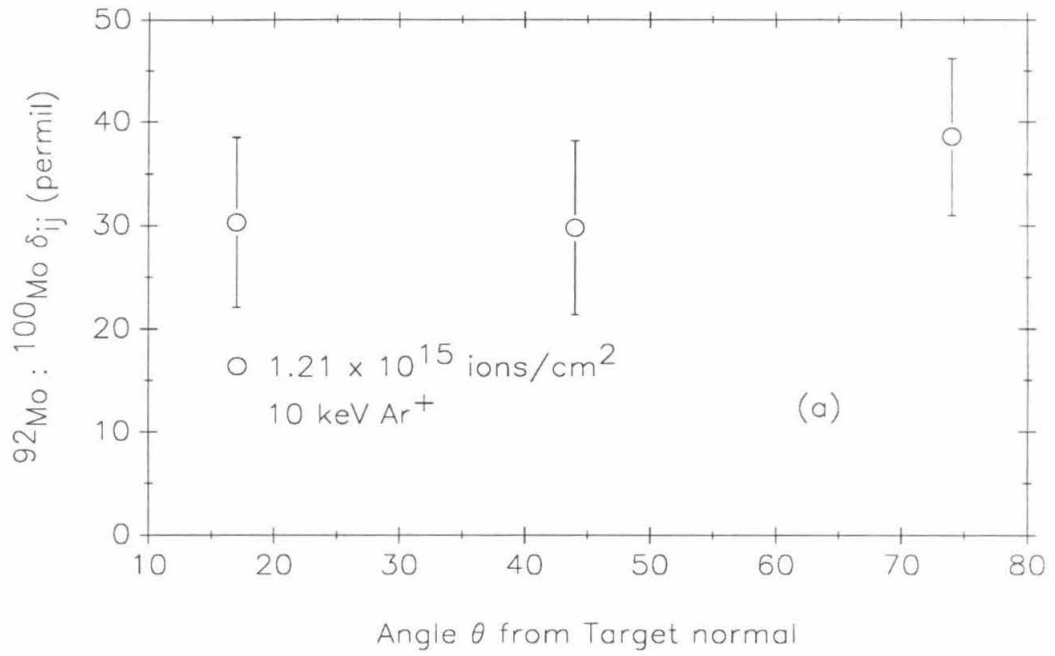
50
40
30
20
10
0
10
20
30
40
50
60
70
80
^{92}Mo : ^{100}Mo δ_{ij} (permil)
O 1.21 x 10^{15} ions/cm^2
10 keV Ar$^+$
(a)
Angle θ from Target normal

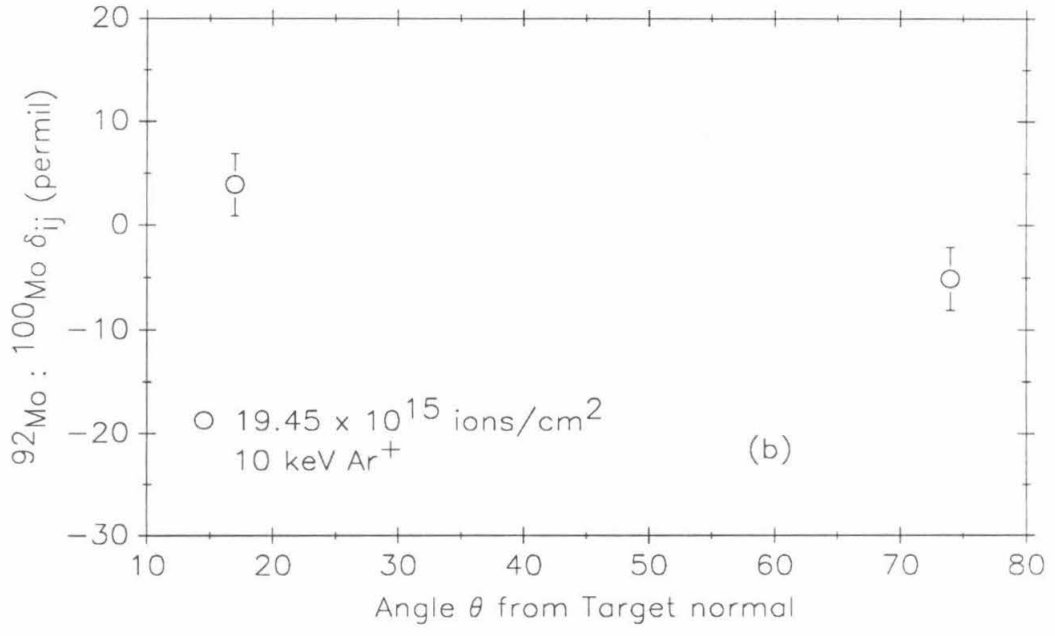
20
10
0
−10
−20
−30
10
20
30
40
50
60
70
80
^{92}Mo : ^{100}Mo δ_{ij} (permil)
O 19.45 x 10^{15} ions/cm^2
10 keV Ar$^+$
(b)
Angle θ from Target normal

Figure 3.8

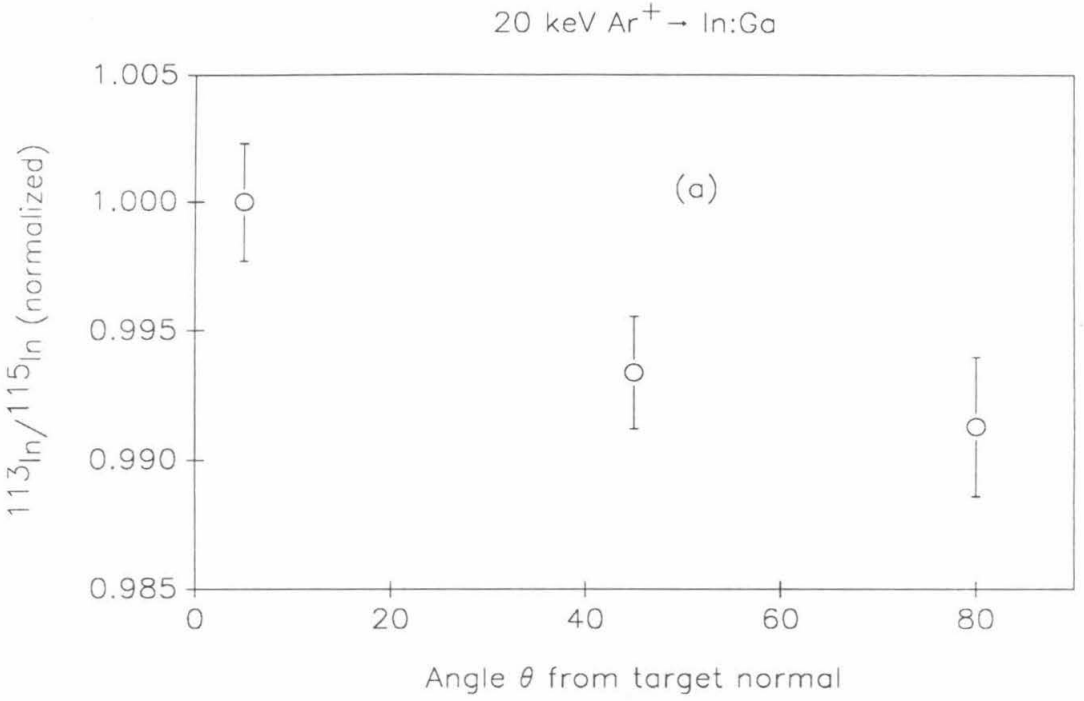
20 keV Ar+ → In:Ga
1.005
1.000
0.995
0.990
0.985
(a)
113In/115In (normalized)
0
20
40
60
80
Angle θ from target normal

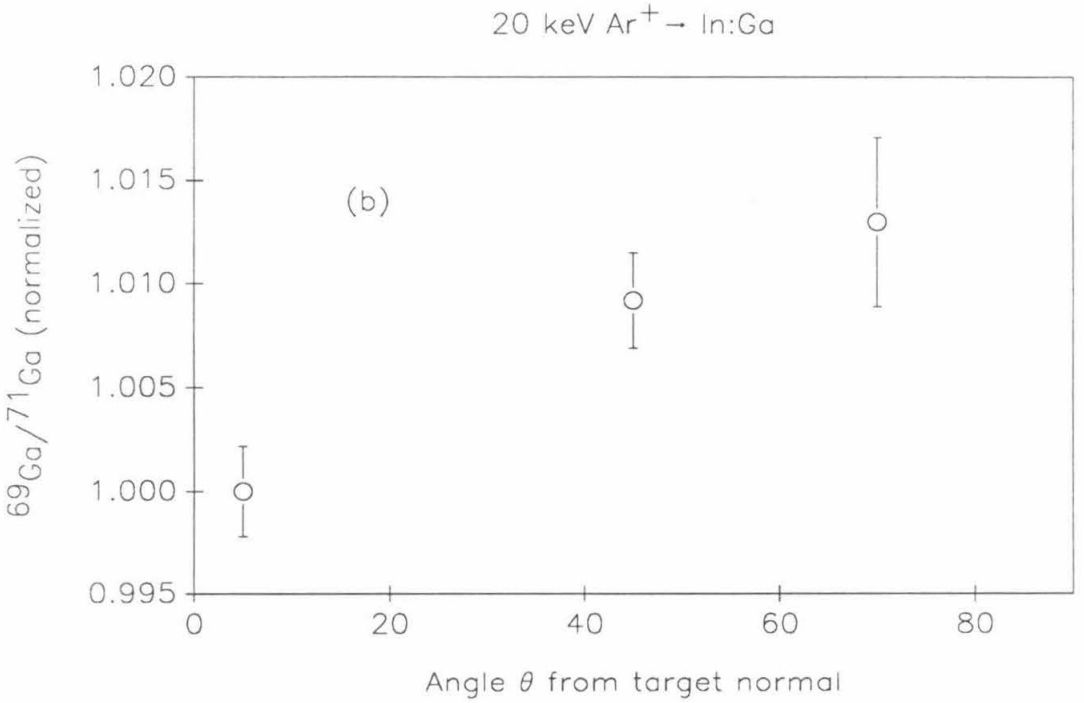
20 keV Ar+ → In:Ga
1.020
1.015
1.010
1.005
1.000
0.995
(b)
69Ga/71Ga (normalized)
0
20
40
60
80
Angle θ from target normal

Fig. 4.1

Simulation Results

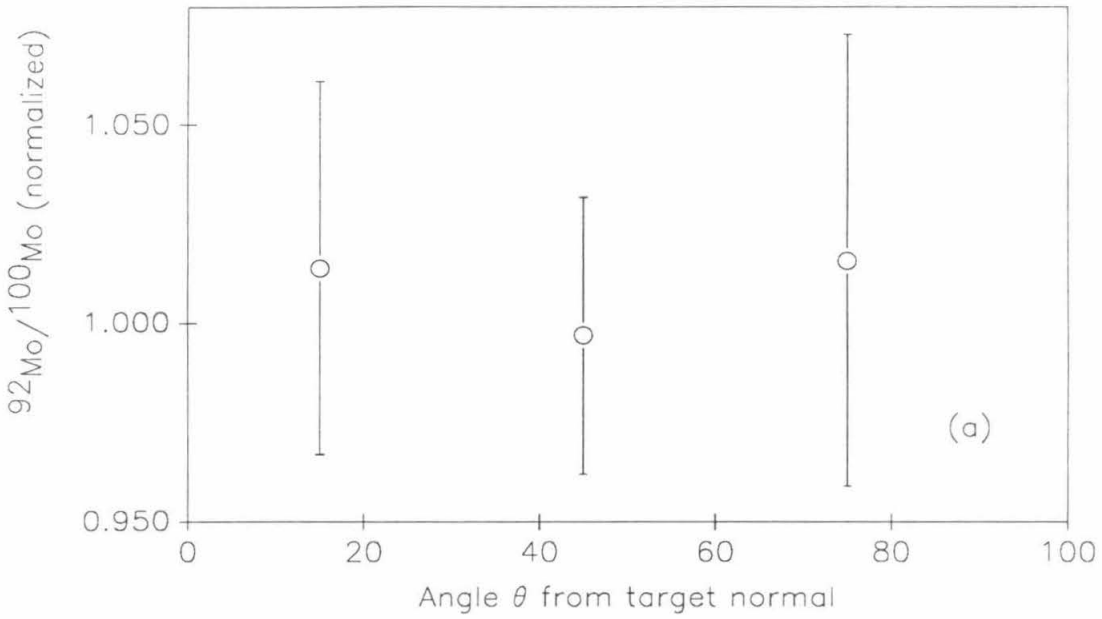

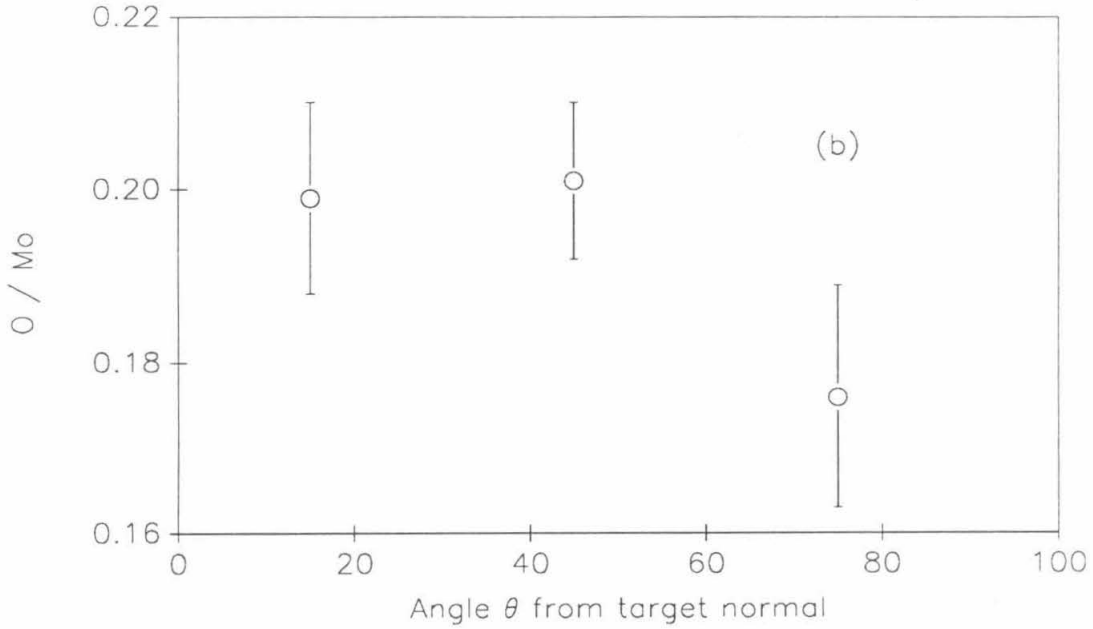

Figure 5.1

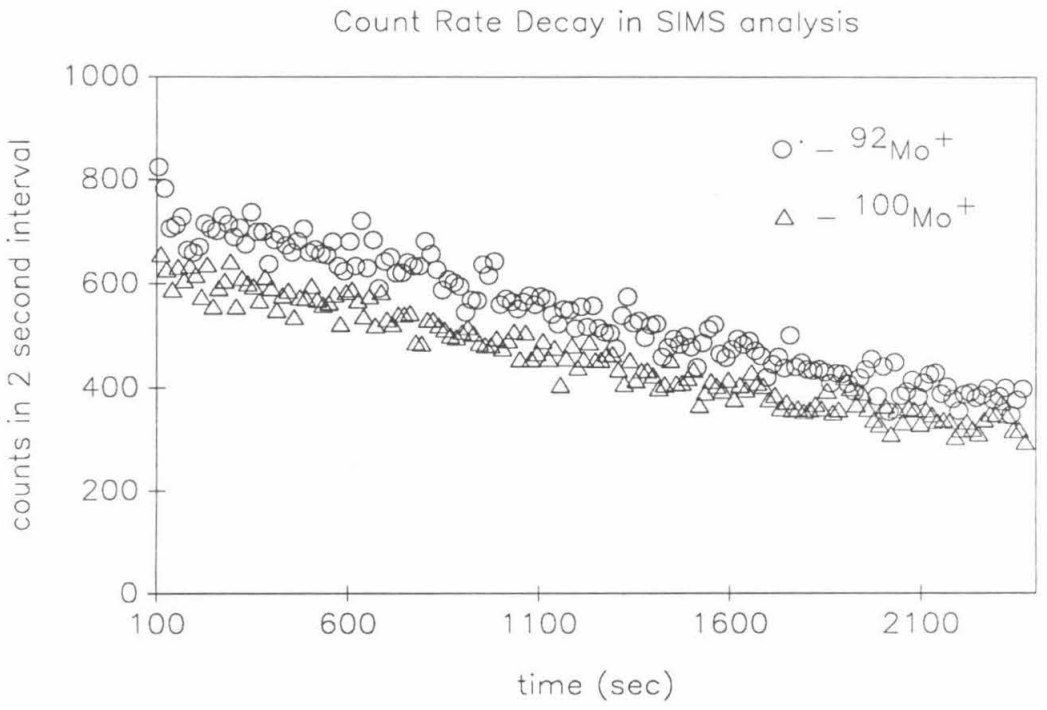
Count Rate Decay in SIMS analysis
1000
800
600
400
200
0
counts in 2 second interval
○ – $^{92}Mo^+$
△ – $^{100}Mo^+$
100
600
1100
1600
2100
time (sec)

Fig. B.1

Table 3.1 Measured enrichments of isotopic ratios.[c]

Projectile	Fluence Range ($\times 10^{15}$ ions cm^{-2})	Angle[a] (degrees)	δ_{ij}^{b} (permil)
10 keV Ar^+	0–1.21	17	30.3 ± 8.2
$^{92}Mo/^{100}Mo$	"	44	29.8 ± 8.4
	"	74	38.6 ± 7.6
	1.21–3.65	17	31.0 ± 3.5
	3.65–7.31	17	14.7 ± 3.1
	7.31–19.45	17	3.9 ± 3.0
	"	74	-5.1 ± 3.0
5 keV Ar^+	0–1.22	17	38.1 ± 6.4
$^{92}Mo/^{100}Mo$	"	44	37.7 ± 7.1
	"	74	20.5 ± 8.1
	2.43–4.86	17	24.6 ± 3.4
	"	74	23.1 ± 4.4
	4.86–8.50	17	12.0 ± 3.3
	8.50–20.63	17	3.8 ± 2.7
	"	44	1.2 ± 4.0
	"	74	-10.4 ± 3.1
10 keV Xe^+	0–0.61	17	29.1 ± 5.1
$^{92}Mo/^{100}Mo$	"	44	15.0 ± 8.3
	"	74	16.8 ± 8.6
	0.61–1.82	17	32.3 ± 3.4
	1.82–3.66	17	28.5 ± 3.5
	3.66–9.74	17	18.1 ± 2.5
	"	44	19.6 ± 4.2
	"	74	-6.5 ± 3.2

a. Polar angle in the sputtering geometry, measured from the target normal.

b. Average enhancement over the indicated fluence range, calculated with respect to the steady-state isotope ratio at angles close to the target normal. Errors shown are $\pm 2\sigma$. They *do* include the uncertainty in the normalization factor and an additional effective 2.0‰ uncertainty has been folded in to account for overall reproducibility [20].

c. Although most of this data is new, some did appear previously in a slightly different form [20].

Table 3.1 cont'd: Measured enrichments of isotopic ratios.[c]

Projectile	Fluence Range ($\times 10^{15}$ ions cm^{-2})	Angle[a] (degrees)	δ_{ij}^{b} (permil)
5 keV Xe^+	0–0.30	17	52.7 ± 5.3
$^{92}Mo/^{100}Mo$	"	31	50.7 ± 5.6
	"	44	42.4 ± 5.3
	"	60	24.3 ± 5.5
	"	74	22.2 ± 6.5
	0–0.61	17	45.8 ± 4.1
	"	31	46.8 ± 4.4
	"	44	30.5 ± 4.8
	"	60	22.6 ± 6.5
	$0–1.0 \pm 0.3$	17	35.5 ± 4.3
	"	31	33.5 ± 5.0
	"	44	26.5 ± 4.6
	"	60	15.3 ± 5.2
	"	74	10.7 ± 5.3
	0.61–1.82	17	41.0 ± 4.2
	"	44	26.2 ± 4.0
	"	74	28.9 ± 9.7
	1.82–4.29	17	36.1 ± 3.8
	"	44	21.3 ± 4.8
	"	74	16.3 ± 4.2
	4.29–7.93	17	18.6 ± 4.5
	"	44	11.8 ± 4.1
	"	74	-7.2 ± 3.7
	7.93–20.05	17	0.0 ± 4.7
	"	31	12.2 ± 2.8
	"	44	-2.5 ± 4.3
	"	60	-2.9 ± 3.2
	"	74	-25.1 ± 3.1
20 keV Ar^+	6.47mC		
$^{113}In/^{115}In$		5	0.0 ± 2.3
		46	-6.6 ± 2.2
		80	-8.7 ± 2.7
20 keV Ar^+	6.47mC		
$^{69}Ga/^{71}Ga$		5	0.0 ± 2.2
		46	9.2 ± 2.3
		70	13.0 ± 4.4

abc. See notes on previous page.